1-1-2013

Enhanced Spontaneous Emission And Spectral Analysis Using Waveguide Based Devices.

Pradeep Kumar
Wayne State University,

ENHANCED SPONTANEOUS EMISSION AND SPECTRAL ANALYSIS USING WAVEGUIDE BASED DEVICES.

by

PRADEEP KUMAR

DISSERTATION

Submitted to the Graduate School

of Wayne State University,

Detroit, Michigan

in partial fulfillment of the requirements

for the degree of

DOCTOR OF PHILOSOPHY

2013

MAJOR: ELECTRICAL ENGINEERING

Approved by:

_____

Advisor Date

_____

_____

_____

_____

DEDICATION

Dedicated to

To my wife, Swati Singh, and son, Uday Singh, who I love endlessly.

&

To my mother, Shyamveeri and Krishna, my inspiration for strength, kindness and love.

ACKNOWLEDGMENT

First and foremost, I would like to thank my advisor Dr. Ivan Avrutsky for all the discussions, his valuable advice and guidance. I extend my thanks to Dr. Pepe Siy, Dr. Cheng-Zhong Xu, Dr. Yong Xu, Dr. Amar Basu, Dr. Mark Cheng and Dr. Xiaoyan Han for their advice and support throughout my study at Wayne State University. I thank Dr. Boris Nadgrony for being very kind and agreeing to be part of my dissertation committee. I thank Monika K. Weidmann, and Dr. Charles H. Winter from Chemestry Department for their collaboration on fabrication of waveguide. I also sincerely thank National Science Foundation (NSF) and Center for Photonics and Multiscale Nanomaterials (CPHOM) for the financial support through grant NSF STTR Phase I and Phase II grant number 0924702 and NSF/C-PHOM grant number DMR 1120923.

I would like to take this opportunity to thank all those without whose help this research would not have been possible - particularly I would like to mention Dr. Zhixian Zhou for his discussion and assistant on AFM. I specially thank Pennsylvania State University nano fabrication staff for the trainning and assistant in fabrication work involving ebeam lithography. I thank Brent C. Bergne, David Cook, and Daphnie Chakran from Spectrum Scientific Inc for their collaboration on Microspectrometer and all their friendly discussion and help.

Also, I would like to thank fellow graduate students in the Opto-Electronics Research Group, Sabarish Chandramohan, Mohammad Hossain, Gurinder Bawa, Eray Hasan and also former graduate students Srikant Raman, Aman Sangwan, Bala chandar for their help and co-operation. I also thank Cynthia Lee Sokol and PhD Office staff for their friendly nature and extreme patience. I extend my thanks to the ECE

department secretary, Dories R. Ferrise for her help.

My special thanks to my friend and fellow graduate student, Gurbindra Khara, Rahul Arora, and Ajay Kumar for their ever good company, cheering and support during the final days.

I thank all my friends and family - especially my Father (Shri Chand), Brother (Kuldeep), and Sisters (Pooja, Suraksha, and Arti) for the love, encouragement and good spirits.

PREFACE

In this dissertation, I present my work on spontaneous emission and spectral analysis using optical waveguide. The first part of the dissertation discusses the fabrication and characterization of optical waveguide. In the Second part of dissertation, I presented the fabrication of microspectrometer using planar waveguide. In final part of my dissertation, I have discussed coupling efficiency of a quantum emitter on top of a planar waveguide.

Chapter 1 begins with the introduction of waveguide, and their applications in various field of science & technology. It describes the different technique of waveguide deposition and why atomic layer deposition technique is better for waveguide deposition. It also discusses different kind of microspectrometers and why the diffractive optical element based microspectrometer has an advantage over other micropectrometers. Final part of chapter 1 introduces the idea of an excited atom or molecule near planar waveguide and its comparison with other fluorescence based microscopy. It explains how to optimize the coupling efficiency of an excited atom or molecule near planar waveguide.

Chapter 2 describes the high index step planar waveguide with low propagation loss. In this chapter, surface roughness and uniformity of high index film was investigated by atomic force microscope and reflection spectrum in a wide spectral range respectively. The propagation losses was measured by collecting light along the guided path.

Chapter 3 describes the fabrication of microspectrometer by e-beam lithography. This chapter also discusses the resolution of the devices in visible spectral range and comparison with other microspectrometers.

Chapter 4 is about the coupling efficiency of an exited atom placed near to a waveguide. In this chapter, I have presented the effect of refractive index of film, position of quantum emitter with respect to the waveguide and dipole matrix element on coupling efficiency of a quantum emitter near planar waveguide.

Sincerely,

Pradeep Kumar.

TABLE OF CONTENTS

LIST OF TABLES

LIST OF FIGURES

CHAPTER 1

Introduction

Waveguide is one of the basic component of integrated optics and optoelectronics [1–4]. It consists of a substrate and a high refractive index thin film which confines and directs light. Strong light confinement in a thin film is needed for many applications, i.e. in sensor applications strong confinement provides high sensitivity and in integrated optical circuits that substitute micro-electronic circuits etc.

Optical waveguide can be classified according to their geometry, mode profile, and refractive index distribution. By geometry of the cross - section, there are different types of waveguide; planar waveguide, strip waveguide, rib waveguide, and photonic crystal waveguide etc. By mode structure: single-mode and multi-mode waveguide. By refractive index distribution: step and gradient index waveguide. Waveguides have many application such as in the field of bio-chemical sensor, modulators, resonators, and amplifiers [5–8] etc.

In this disertation we will exploit high index step waveguide, optical waveguide as microspecrometer, and enhanced spontaneous emission near waveguide.

1.1 Large Index Step Waveguide By Atomic Layer Deposition

Strong confinement depends upon many parameters, out of which the large index step between core and cladding are most important. The silicon-on-insulator(SOI) is the best choice for high index step between film (silicon, refractive index = 3.45) and substrate (SiO_2, refractive index = 1.45). Also it is compatible with comple-

mentary metal oxide semiconductor (CMOS) fabrication process. Besides all benefits, SOI is not transparent in visible range.

Other materials that are mainly used in construction of waveguides include polymers, tantalum oxides(TaO_2), titanium oxides(Ti_2O_2), magnesium oxide(MgO), silicon dioxide(SiO_2), aluminium oxide (Al_2O_3), and hafnium oxide (HfO_2). Polymers, magnesium oxide(MgO), and silicon dioxide(SiO_2) based waveguides have low index step. Tantalum oxides (TaO_2), titanium oxides (Ti_2O_2), aluminium oxide (Al_2O_3), and hafnium oxide (HfO_2) based waveguides have high index step.

Aluminum Oxide (Al_2O_3) is a widely used waveguide material. It is cost effective and the raw materials from which it is made are widely available unlike other high index step materials. Due to the dielectric and electrical properties, Al_2O_3 is used as an optical material in thin film devices. With respect to SiO_2, it has a relatively higher index allowing for light to be confined very well in the waveguide [9]. The most critical optical waveguides properties are effective refractive index and optical loss. The transmission window of Al_2O_3 ranges from 200 nm to 9 μm and the refractive indices also range between 1.64 and 1.86.

Fabrication of nano-structures using techniques such as focused ion beam (FIB) milling for use in an integrated photonic devices is more possible in Al_2O_3 waveguides [10], because Al_2O_3 waveguide is not greatly affected by the implantation of Ga ion. It is unlike SOI waveguide that is much more affected by Ga ion implantation. Thus a reflection grating is easily realizable on an Al_2O_3 channel waveguide [11].

Optical waveguide mostly fabricated by plasma enhanced chemical vapor deposition (PECVD), thermal vapor deposition, sol-gel, and pulsed layer deposition etc. The atomic layer deposition waveguide films have not been studied extensively in the literature, perhaps because of slow growth rate. We investigated optical and waveguide properties of Al_2O_3 films on silicon and soda lime glass substrate deposited by

atomic layer deposition.

1.1.1 Fabrication of Al_2O_3 Waveguide

Waveguides are fabricated by many techniques such as, plasma enhanced chemical vapor deposition (PECVD), thermal vapor deposition, atomic layer deposition (ALD), and sol-gel [13–17] etc. The atomic layer deposition [14–16] gives high thickness uniformity due to its self-limiting nature, which reduces the losses due to surface imperfection. The film growth in ALD occurs through layer by layer deposition resulting in atomically smooth surface.

Aluminum oxide films made by atomic layer deposition usually have a higher refractive index compared to those made by evaporation techniques. Low refractive index with porosity leads to higher optical losses usually in the range of 15 to 25 dB/cm which can be attributed to the varying porosity throughout the amorphous aluminum oxide matrix. On the other hand, films deposited by sputtering have refractive indices in the range of 1.57 to 1.7, which is relatively higher when compared to films produced by evaporation techniques and subsequent loss between 5 to 20 dB/cm [18]. Judging from the above films, it is evident that films with lower refraction indices often have higher losses and are more likely to have porosity.

Aluminum oxide films are usually used in construction of various types of waveguides that find application in a number of fields such as microelectronics and optics [19]. This is primarily because Al_2O_3 films have a relatively high reflective index. Amorphous Al_2O_3 has very promising optical properties especially for planar waveguides. Atomic deposition produces high index aluminum oxide films that usually have indices ranging from 1.64 to 1.86 with and optical loss is between 1 to 10 dB/cm at 632.8 nm.

1.1.2 Optical and Waveguide Properties of Al_2O_3 Waveguide

The Al_2O_3 thin film is transparent in 200 nm to 9μm wavelength range and most of the optical properties were investigated in spectral range 400 nm - 1000 nm [14, 20]. The refractive index varies from 1.66 to 1.64 in spectral range of 400 nm - 800 nm [14] and thorough investigation is needed to get refractive index of Al_2O_3 in wide spectral range. Since optical properties of thin film deposited by atomic layer deposition depends upon the substrate, as reported by Kim et al. [14], error should be investigated thoroughly too.

We have measured a refelction spectra of Al_2O_3 thin film in spectral range 400 nm to 1800 nm. The measured reflection spectra then fit to the theoretical reflection spectra. The film refractive index and film thickness was calculated from this fit and the error was investigated by calculating mean squared error (MSE).

1.2 Waveguide Based Microspectrometer With a Computer Generated Diffractive Optical Element

Spectrometer by definition is a device which resolve wavelength by angular or spatial separation. Spectrometers have three basic components: a diffractive element, focusing or collimating, and a detector or detectors array. Spectrum of light can be realized by using optical filters [21, 22] and diffractive gratings [22–25]. The applications of spectrometers are spread in many fields.

Bench top spectrometer have been used in many areas, i.e. dye industry, gems industry, paint industry, chemistry and biology laboratory, defense, medicine, environmental studies, and many other areas. Absorption spectrometry is used to determine the presence of elements in chemicals which cannot be measured directly. Emission spectrometry is used to record the spectrum of atoms and can be compared with

absorption spectrum.

Infrared spectrometer finds applications in science, industry, and medicine. Spectrometers that operates in ultraviolet-visible (UV - VIS) region with wavelengths between 280 nm- 850 nm spectrum finds applications in colorimetry, fluorescence based techniques, and atomic absorption spectroscopy. For the analysis of signals in surface enhanced Raman spectroscopy (SERS) and surface Plasmon resonance (SPR) spectroscopy, ultraviolet-visible spectrometers are quite helpful. Ultraviolet-visible spectroscopy based instruments can make use of cost-effective and readily available detectors and sources. Miniature or micro-spectrometer are required in many areas, where moving a bench top spectrometer is not possible, i.e. space, marine study etc.

1.2.1 Microspectrometer

Microspectrometers can be used at places which were once limited to the laboratory. In situ studies are required in many areas where collection and transportation of the sample effect the result [26, 27]. Microspectrometer offers ability to conduct research in field and avoid false result due to transportation. Microspectrometers are being used on site for chemical analysis, blood analysis and for many other applications in biology and chemistry [28]. Microspectrometers have been developed for ultraviolet-visible [21–25, 29–31] , and infrared regions [32–34].

Based on their principle, microspectrometers can be classified as Fabry-Perot filter [21,31], acousto-optical tuneable filter (AOTF) [29,35], Fourier transform [30,32], and grating- based [22–25, 33, 34] spectrometer etc. Fabry- Perot filter and Fourier transform based micro-spectrometer contains movable part. The draw-backs in Fabry-Perot filter based microspectrometer are: fabrication of mirror with appropriate flatness and reflectivity, high voltage needed to tune the movable mirror, and to fabricate two mirrors parallel to each other.

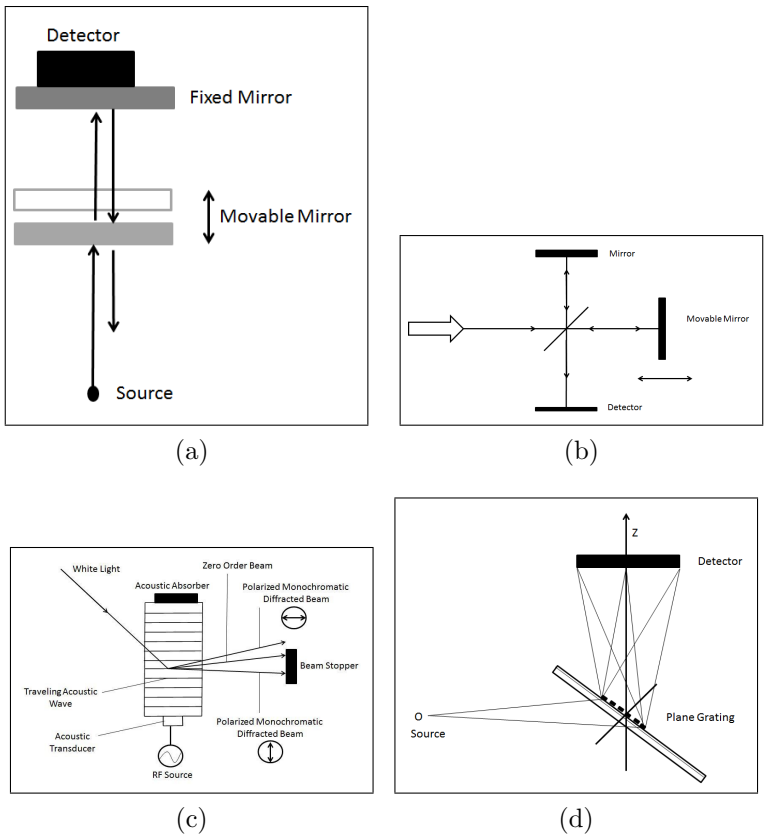

Figure 1.1: Schematic view of the. (a) Fabry-Perot filter, (b) Fourier transform, (c) Acousto-optical tuneable filter (AOTF), and (d) Grating based microspectrometer.

The limitations of Fourier transform based microspectrometer is that it consists of movable mirrors. Acousto-optical tunable filter (AOTF) based microspectrometer doesn't require any movable part and it consists of a crystal which acoustic waves are used to separate a single wavelength of light. But acousto-optical tunable filter (AOTF) based microspectrometer works more as a monochromator rather than spectrometer. A grating based microspectrometer doesn't have any movable part and works as a spectrometer. The performance of grating based microspectrometer is directly related to the quality of grating and that can be achieved by careful design of the grating. The grating based microspectrometer has an advantage over

Fabry-Perot filter based, acousto-optical tunable filter (AOTF) based, and Fourier transform based microspectrometer.

1.2.2 Diffractive Optical Element Based Microspectrometer

A diffractive optical element can perform spectral dispersion and focusing of light. Diffractive optical element based microspectrometer provides quick read out as compared to optical filter based microspectrometer. A diffractive optical element works on the principle of diffraction. Primary wavefront interfere with secondary wavefront and generate diffraction pattern. The grating act as a multiple silts, with grooves arrangement on substrate. The density of grooves provides the approximate calculation of spectral resolution. For example if the total number of grooves are 500 in a diffraction grating than it will provide 1 nm spectral resolution at 500 nm wavelength.

A recent review on state of art optical spectrometer [22] states that larger size of spectrometer provide good spectral resolution and smaller size of device provide worse spectral resolution. But this is not the case today, with the development of technology any desired size of grating can be realized. The best reported resolution for microspectrometer of size 10 or 20 mm in visible range is from 5 nm to 10 nm for both optical filters and diffractive optical element based design. Ref [23] demonstrate a planar waveguide based microspectrometer with a focusing grating and gives 10 nm resolution in visible range 350 nm - 650 nm. Ref [25] demonstrate a microspectrometer based on planar reflection grating and gives 5 nm resolution in visible range 510 nm - 610 nm. Ref [30] is very compact but provides 6 nm spectral resolution in visible range 400 nm - 800 nm and ref [34] provides 0.07 nm spectral resolution but with a spectral range of 14 nm. There is a trade off between size of spectrometer, spectral resolution, and spectral range. As the size of spectrometer reduces, spectral resolution gets worse.

Also, as the spectral resolution gets better, spectral range becomes smaller.

This is clear that there is need of microspectrometer with good resolution in visible spectral range for many applications. We have proposed a novel design to get better resolution in visible spectral range than the existing devices. Careful designing of diffractive optical element will provide good spectral resolution in visible spectral range. The primary result with diffractive optical element was shown by our group [36, 37]. In experiment, plain grating was used for diffraction and the focusing of diffracted light was achieved by using plan - convex lens. The spectral resolution was varied from 0.3 to 4.6 nm within the wavelength range of 472 nm - 666.0 nm. To make it integrated microspectrometer further development was done by replacing plan grating to chirped grating. The chirped grating provide diffraction and focusing of diffracted light. With the help of chirped grating the output light is aimed and focused at a distance from waveguide surface. Wavelength and order of guided mode decides the location of focal point. Chirped grating based microspectrometers have a edge over focusing and resolving, a range of wavelengths with the help of common optical element.

The chirped waveguide grating was used in optical communications. The chirped waveguide grating as a diffractive element in spectrometer was first studied by our group. The design consists of chirped waveguide grating integrated into the single mode planar waveguide. Chirped waveguide grating was fabricated on top of HfO_2 film on quartz substrate and the design was done for spectral range from 425 nm to 700 nm. The spectral resolution was 2 nm in spectral range between 424 nm - 700 nm. Figure (1.2) shows schematic view of chirped waveguide grating based microspectrometer.

The CMOS camera was used to record the image. To find out the full width half maximum, matlab curve fitting toolbox was used to fit recored intensity. The

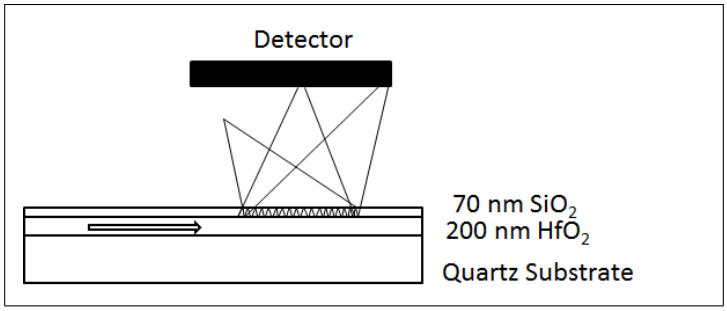

Figure 1.2: Integrated chirped waveguide grating based micro-spectrometer.

fabrication and experiment was done in collaboration with Spectrum Scientific Inc, Irvine, California.

1.3 Enhanced Spontaneous Emission Near Waveguide

A quantum emitter such as an atom or a molecule undergoing spontaneous transition from an excited to ground state emits light into available electromagnetic modes. It has been recognized by Purcell [38] that spontaneous emission is not only a property of the emitter but it is also strongly affected by the environment. One of the processes of spontaneous emission is fluorescence, and the emitter is an ion, atom or molecule. The emission from quantum emitter can be captured and used as an optical sensor. Based on the optical structures, optical sensors can be classified as total internal reflection fluorescence based sensors, optical ring resonator based sensors, and optical waveguide based sensors etc. A total internal reflection fluorescence based sensor [39] uses an evanescent wave to selectively illuminate and excite atom or molecule in a restricted region of the specimen immediately adjacent to the interface and the fluorescence was captured by the optical microscope.

Optical ring resonator based sensors [40, 41] are also based on total internal reflection of light along curved boundary between ring and its surrounding. The

guided mode spectral position is directly related to the effective refractive index(n_{eff}) by $\lambda = 2\pi r n_{eff}/m$, where λ is resonant wavelength, r is the ring outer diameter and m is an integer. The effective refractive index changes when a quantum emitter near to the optical ring modifies the effective refractive index. The advantage of optical ring resonator based sensors is sensing performance, while size of sensing area is much less than the total internal reflection based sensors. Since the size of optical ring resonator is near about 100 μm x 100 μm, so to deliver atom or molecule to the sensing area micro-fluidic channel needs to be fabricated. The integration of optical ring resonator and fluidics is very difficult.

Optical waveguide based sensors also works on total internal reflection and the guided light in guiding layer goes under total internal reflection at guiding layer-cladding interface. The evanescent wave at upper guiding layer-cladding interface interact with analyte. In conventional waveguide, the lower cladding layer or substrate has higher refractive index than upper cladding layer, thus the guided mode has less intensity sitting in upper cladding layer and this effect the sensor performance.

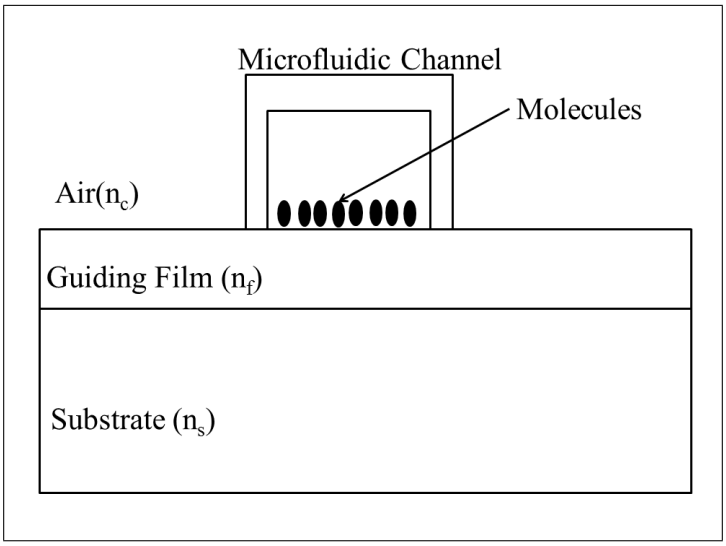

Figure 1.3: Proposed design for optical waveguide based sensor.

There is a need of a design, which will be compatible with fluidics. Micro-fluidic channels will ease the sample injection and drainage. Also it will reduce the analyte or sample consumption. The optical planar waveguide surface is very appropriate for micro-fluidics channel fabrication. The integration of micro-fluidic channel and optical waveguide will help to realize the lab-on-chip system and can be used out side the lab, i.e. hospitals, clinics, and for on-site analysis. Figure (1.3) shows the proposed design for optical waveguide based sensor with micro-fluidic channel. A thorough investigation is needed for spontaneous emission from quantum emitter captured by optical waveguide. Instead of analyte excited by evanescent wave, analyte was excited by external source. The theoretical model was developed to estimate light captured by waveguide.

If a quantum emitter placed near to the waveguide boundary, then decay can occur in either of the following two ways: guided mode, and radiation mode. The likelihood of these two ways is dependent on the particulars of the system [42, 43]. The expression of the rate of spontaneous emission could be in terms of the zero-point fluctuations of the electromagnetic field at the atom's location. The fluctuations of the local zero-point field are dependent on the modes of electromagnetic field strengths as well as the photon density of the states [44]. Since the modes of the electromagnetic fields are highly dependent on the electromagnetic and configuration characteristics of the materials, the rate of spontaneous emission could either be reduced or increased and this depends on the electric characteristics of the environment of the atom [45,46]. Previous experimental studies have shown that when atoms are put in a cavity, the rate of spontaneous emission is different when compared to the value in free space [47].

In general, when a dielectric waveguide is present, two dissimilar sorts of electromagnetic waves may be identified: (i) waves that have been trapped by the waveguide and therefore restrained to its nearness and interior and is capable of propagating

along its length; and (ii) waves, which at lengthy distances act as free waves. They are altered because of the processes of scattering [46, 48, 49].

Urbach and Rikken [44] applied quantum electrodynamics in calculating the zero-point fluctuations of the electromagnetic field. They also applied it in calculating the spontaneous rate of emission from a dielectric non-absorbing film that had been circumscribed by two non-absorbing dielectric half spaces. These half spaces were of arbitrary refractive indices. For dielectric film in this experiment, the set of modes comprised of radiation modes. The modes are evanescent in the two dielectric half spaces.

In evaluation of spontaneous emission rate it is often assumed that the atoms or molecules are randomly oriented in space. Both transverse electric (TE) and transverse magnetic (TM) modes of the film then collect the radiation. In some rare cases the assumption of random orientation may not be justifiable. The specific adsorption relies on chemical bonds created between the chemical that functionalizes the surface and particular radicals of the analyte molecules. This may lead to preferential orientation of the adsorbed analyte molecules in space. For instance, long molecules may all get attached to the surface by a certain end resulting in their orthogonal orientation with respect to the surface. If the dipole matrix element of the transition of interest happens to be orthogonal to the surface, then emitted radiation can only be coupled to the TM modes of the film.

This case is interesting because the radiation into free space modes propagating close to the normal to the surface is weak (an oscillating dipole does not radiate along the dipole direction) leading to improved efficiency of collecting the radiation into the guided mode. When evaluating the coupling efficiency, we consider the cases of random orientation, dipole matrix element orthogonal to the surface, and dipole matrix element random but parallel to the surface.

CHAPTER 2

Characterization of Waveguide Prepared by Atomic Layer Deposition of Alumina.

2.1 Fabrication of Al_2O_3 Waveguide

Finding a waveguide material for high index step has been a most crucial part in integrated optics. As mention in chapter 1, high index step leads to strong confinement. The strong confinement provides high degree of integration and allows sharp bending of light. Al_2O_3 is perfect material for waveguide implementation due to its high refractive index and transparency in large range of wavelength.

In our study, we had fabricated Al_2O_3 waveguide in collaboration with Dr. C. Winter from Chemistry Department on silicon and soda lime glass substrate by atomic layer deposition (ALD) technique. Al_2O_3 film is deposited by atomic layer deposition (ALD) on soda lime glass and silicon substrate to form a film with thickness of 400 nm, 300 nm, and 200 nm. The substrate dimensions were approximately 39 mm x 25 mm. The optical properties of Al_2O_3 were investigated in spectral range of 400 nm - 1800 nm. The effective refractive index and propagation loss were measured at wavelength 632.8 nm.

Al_2O_3 films were grown in a Picosun R-75 ALD reactor using trimethylaluminum (TMA) and water [50]. The deposition temperature was 300 C and films with nominal thicknesses of 400, 300, and 200 nm were grown with 4400, 3300, and 2200 deposition cycles, respectively. Each cycle consisted of a 0.1 s TMA pulse, followed by a 3.0 s nitrogen purge, a 0.1 s water pulse, and finally another 3.0 s nitrogen purge.

The surface roughness of the films were measured by atomic force microscope

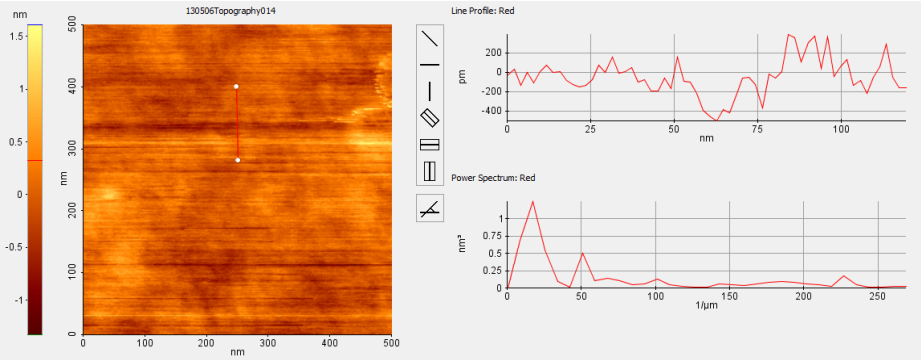

(a)

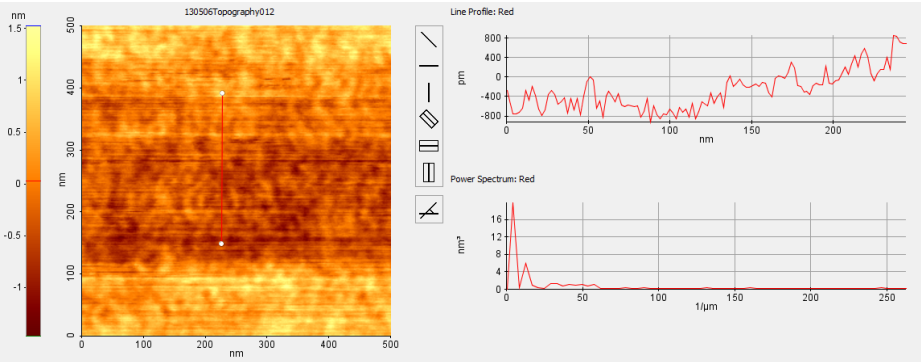

(b)

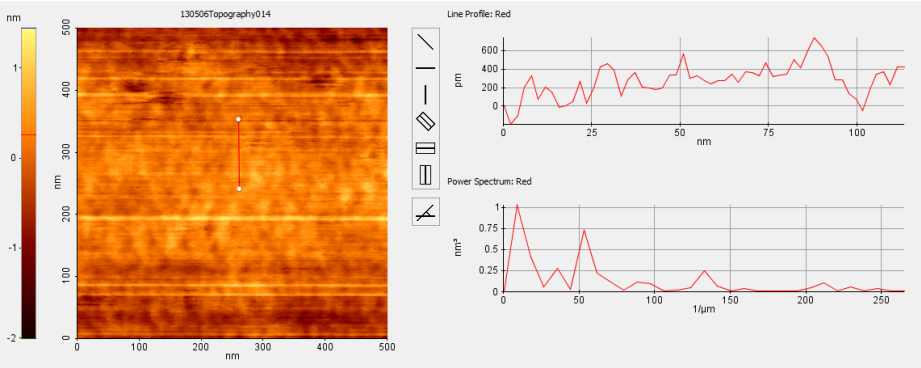

(c)

Figure 2.1: AFM images of (a) 400 nm, (b) 300 nm, and (c) 200 nm Al_2O_3 films.

(AFM). Figure (2.1a), (2.1b), (2.1c) shows the AFM images of 400 nm, 300 nm, and 200 nm. The scanned area under AFM was 500 nm x 500 nm. The surface roughness was measured by selecting a line across the scanned area. For film thickness 400 nm,

300 nm, and 200 nm, the surface roughness was ± 0.2 nm, ± 0.8 nm, and ± 0.3 nm, respectively. The surface roughness of Al_2O_3 by ALD is much better than Al_2O_3 deposited by sol gel [50] . Al_2O_3 film deposited by chemical vapor deposition(CVD) have surface roughness of ±0.3 nm with film thickness of 56 nm [16]. The surface roughness depends upon the film thickness and if film thickness is low surface roughness is low and vice versa. In comparison to chemical vapor deposition, the surface roughness is better in atomic layer deposition.

2.2 Optical Properties

The optical properties of Al_2O_3 film on soda lime glass and silicon substrate were investigated by measuring the reflection spectra at ten different positions on the sample in the spectral range from 400 nm to 1800 nm. Figure (2.2) shows the geometry for calculation of reflection spectrum. The instrument used for this experiment was computer controlled DigiKrom 240 monochromator and halogen lamp as a light source. The incident angle and beam size were 5.6^0 and 0.5 mm, respectively. The reflection spectrum of the film for TE polarization light is given by

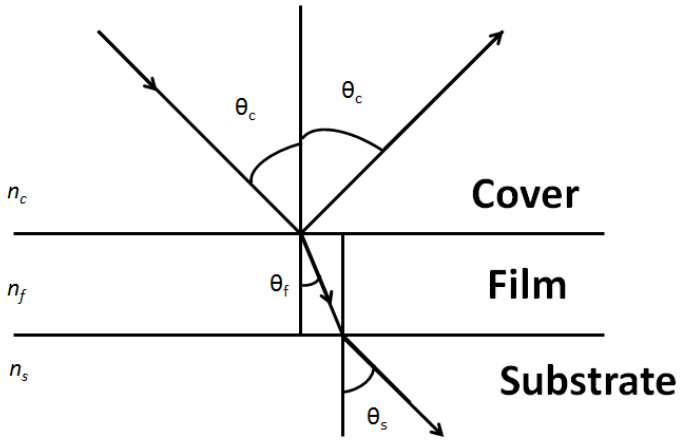

Figure 2.2: Geometry for calculation of reflection spectrum of thin film.

$$R_{calc} = \frac{(g_c - g_f)(g_s + g_f) + (g_c + g_f)(g_f - g_s)exp(2jg_f d)}{(g_c + g_f)(g_s + g_f) + (g_c - g_f)(g_f - g_s)exp(2jg_f d)}, \tag{2.1}$$

$$g_c = \frac{2\pi}{\lambda} n_c cos\theta_c, \tag{2.2}$$

$$g_f = \frac{2\pi}{\lambda} n_f cos\theta_f = \frac{2\pi}{\lambda}\sqrt{{n_f}^2 - (n_c sin\theta_c)^2}, \tag{2.3}$$

$$g_f = \frac{2\pi}{\lambda} n_s cos\theta_s = \frac{2\pi}{\lambda}\sqrt{{n_s}^2 - (n_c sin\theta_c)^2}, \tag{2.4}$$

where n_c, n_s, and n_f are cover, substrate, and film refractive index respectively. θ_c is the incident angle, θ_f is the refraction angle in the film, θ_s is the refraction angle at the film and substrate boundary, λ is the wavelength, and d is the film thickness

Since the measurement is done in such a wide spectral range (400 nm - 1800 nm) that there will be slow drift in the intensity of light source while spectrometer is scanning across the wavelength. To account for intensity drift we have used first order correction in calculated reflection spectrum

$$R_{exp} = R_{calc}(C_0 + C_1\lambda), \tag{2.5}$$

where C_0 and C_1 are adjustable parameter.

Matlab curve fitting toolbox was used for fitting. The experimentally measured reflection spectrum was numerically fit to the calculated reflection spectrum, assuming the Sellmeier formula for Al_2O_3 thin film on substrate. The mean-square differences were minimized between experimental and calculated reflection spectrum angle of incidence, substrate and cover refractive index at corresponding wavelength. The

fitting parameters are Sellmeier coefficients forAl_2O_3, film thickness, C_0, and C_1.

Silicon substrate has higher refractive index compared to the Al_2O_3 thin film. The minima of the reflection spectrum are clearly pronounced. The logarithm of experimentally measured reflection spectrum was numerically fit to the logarithm of calculated reflection spectrum. For soda lime glass sample the experimental measured

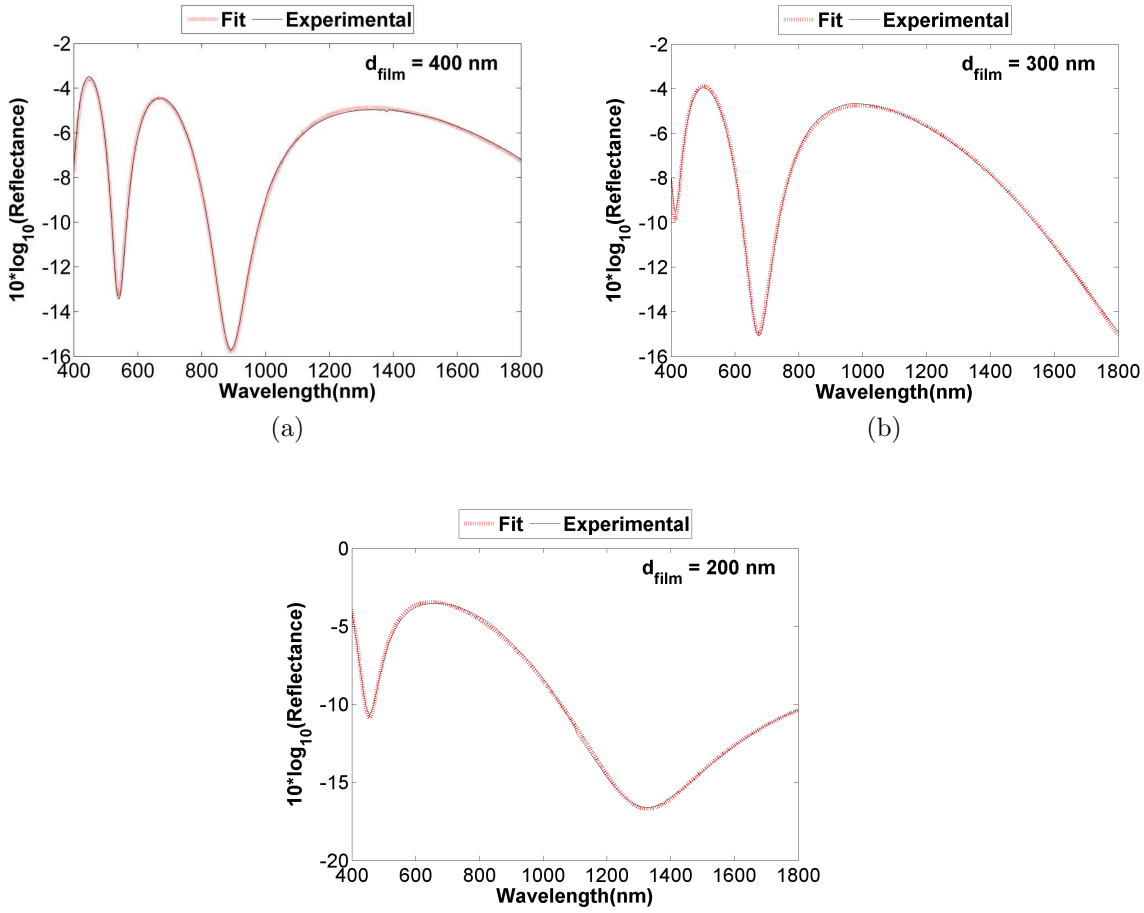

Figure 2.3: Experimental and calculated reflection spectra for Al_2O_3 films on silicon for thickness (a) 400 nm (b) 300 nm and (c) 200 nm.

reflection spectrum was numerically fit to the calculated reflection spectrum. Figure (2.3) and (2.4) show the measured and fitted reflection spectra of 400 nm, 300 nm,

and 200 nm thick Al_2O_3 film on silicon and soda lime glass substrate.

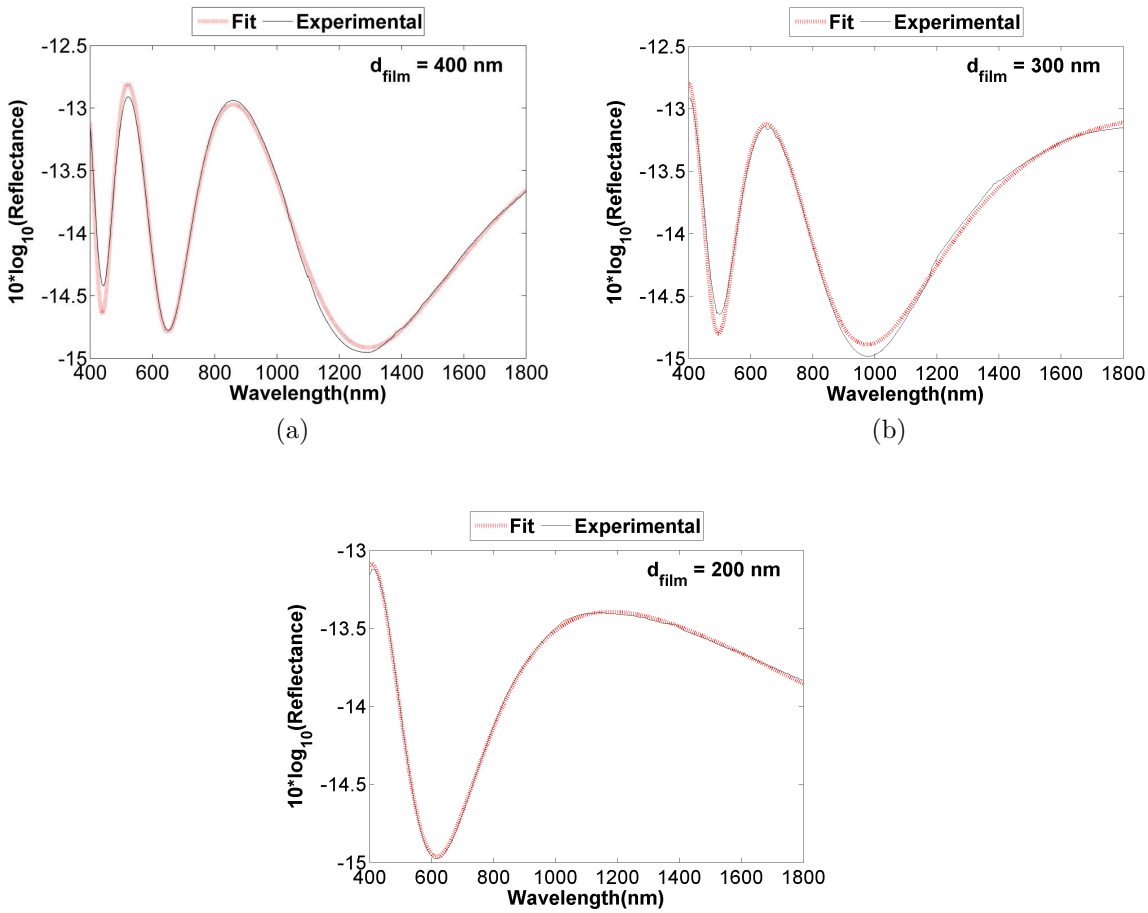

Figure 2.4: Experimental and calculated reflection spectra for Al_2O_3 films on soda lime glass for thickness (a) 400 nm (b) 300 nm and (c) 200 nm.

Equation (2.6) gives mean squared error (MSE) [10] and calculated by

$$MSE = \frac{1}{N}\sum_{j=0}^{N}\left(\frac{R_{exp}^{j} - R_{calc}^{j}}{\sigma^{j}}\right)^{2}, \tag{2.6}$$

where N is the total number of measurements and σ^j is the standard deviation of measured data points.

Tabel (2.1) provides MSE values for Al_2O_3 film on silicon and soda lime glass substrate. Since there is strong anti-correlation between film refractive index and film thickness, so we introduced scaling factor in refractive index and film thickness and contour plot the MSE. The scaling factor introduces controlled error in film thickness and film refractive index to calculate and contour plot. The contour plot for MSE

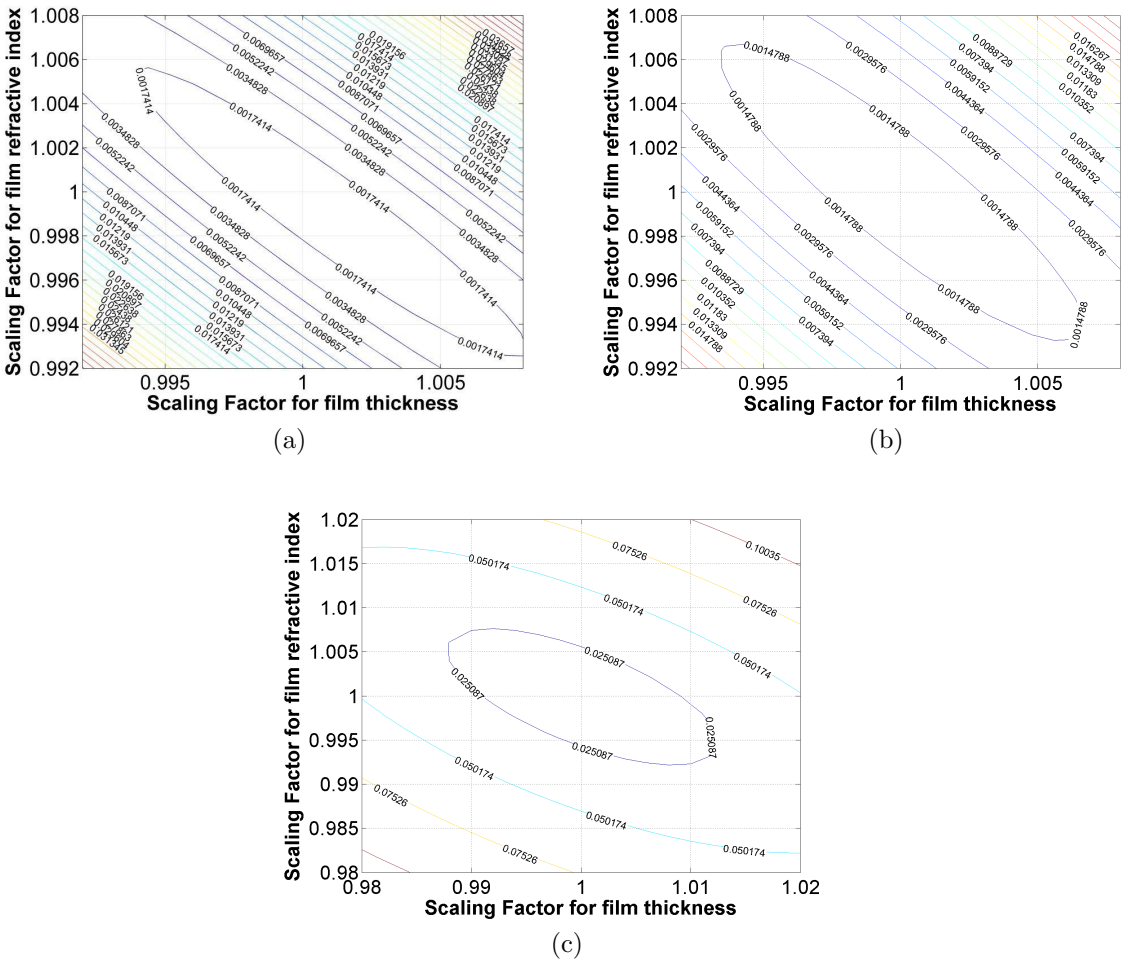

Figure 2.5: MSE variation w.r.t. refractive index and thickness of Al_2O_3 film on silicon substrate (a) 400 nm, (b) 300 nm, and (c) 200 nm thick film.

shows that error is minimum when both the scaling factor is unity and the nearest

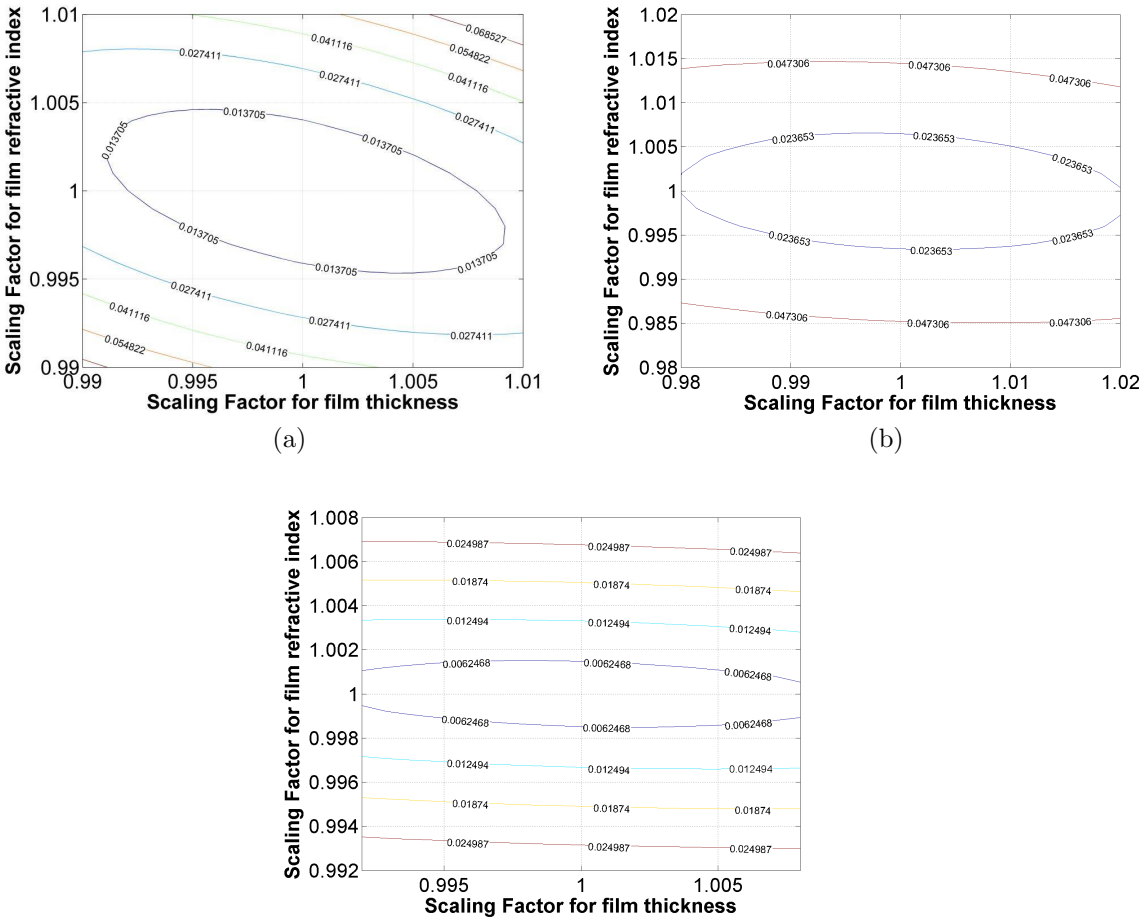

Figure 2.6: MSE variation w.r.t. refractive index and thickness of Al_2O_3 film on soda lime glass substrate (a) 400 nm, (b) 300 nm, and (c) 200 nm thick film.

contour to the minimum corresponds to the doubling the minimum MSE. Figure (2.5) and (2.6) shows the contour plots with respect to the scaling factor in refractive index and film thickness for 400 nm, 300 nm, and 200 nm thick Al_2O_3 film on silicon and soda lime glass substrate.

The refractive index for Al_2O_3 was defined according to the Sellmeier- like dispersion formula

Table 2.1: MSE value for Al_2O_3 films on silicon and soda lime glass substrate.

Substrate	400 nm	300 nm	300 nm
Silicon	0.0008	0.0007	0.0125
Soda lime glass	0.0068	0.0118	0.0031

$$n_f = \sqrt{A_0 + \frac{A_1\lambda^2}{\lambda^2 - \lambda_1^2}}, \tag{2.7}$$

where A_0, A_1, and λ_1 are the Sellmeier coefficients and A_0 account for the contribution of short wavelength absorption to the refractive index at a longer wavelength, A_1 and λ_1 are the relative oscillator strength and resonant wavelength, respectively. Table 2.2 shows the values of these coefficients for Al_2O_3 films on silicon and soda lime glass. The refractive index of Al_2O_3 was calculated by taking average of sellmeier coefficients for given substrate. Figure (2.7) shows the dispersion curves of the refractive index Al_2O_3 film on soda lime glass and silicon substrate.

Table 2.2: Sellmeier coefficients for Al_2O_3 films.

Substrate	Film Thickness (nm)	A_0	A_1	λ_1
Silicon	400	1.31283	1.29987	120.634
	300	1.30451	1.33178	120.0863
	200	1.15965	1.50157	130.091
Soda lime glass	400	1.39185	1.38324	133.829
	300	1.46200	1.25589	149.167
	200	1.42479	1.32544	100.001

The refractive index of Al_2O_3 film on silicon and soda lime substrate has different values. The optical properties of thin films deposited by atomic layer deposition are depend on the substrate [14] and is confirmed by our results too. Our results are in good agreement with those of Raisanen et al. [15] and Ott et al. [16] and higher than the Kim et al. [14]. The reflection spectrum were measured at ten different points and

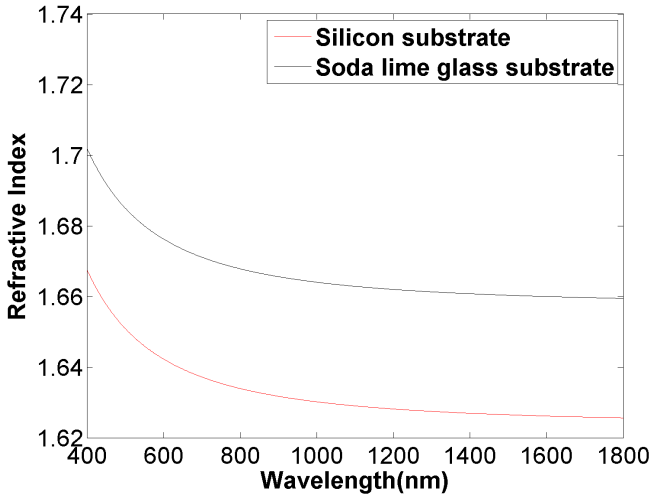

Figure 2.7: Refractive index of Al_2O_3 thin film on silicon and soda lime glass substrate.

thickness of the film was calculated by fitting measured reflection spectrum. Table 2.3 shows the range of film thickness, mean film thickness and the standard deviation in film thickness.

The result shows the uniformity in film thickness over entire substrate. Figure (2.8) shows the thickness of Al_2O_3 film on silicon and soda lime glass substrate.

Table 2.3: Range of film thickness, mean thickness, and standard deviation.

Substrate	Experimental thickness (nm)	Range of film thickness(nm)	Mean thickness (nm)	Standard deviation (nm)
Silicon	400	419-409	413.15	3.00
	300	304-312	307.61	2.22
	200	199-205	202.60	1.43
Soda lime glass	400	380-402	392.27	6.95
	300	290-303	297.85	3.58
	200	180-193	184.08	5.25

2.3 Waveguide Properties

The waveguide properties were investigated for 400 nm, 300nm, and 200 nm thick Al_2O_3 film on soda lime glass. Since Al_2O_3 film on glass substrate behaves like a slab waveguide, the dispersion relation for slab waveguide for TE polarized light is given by

$$m\pi = \frac{2\pi}{\lambda} d\sqrt{{n_f}^2 - {n_{eff}}^2} - tan^{-1}\left(\sqrt{\frac{{n_{eff}}^2 - {n_c}^2}{{n_f}^2 - {n_{eff}}^2}}\right) - tan^{-1}\left(\sqrt{\frac{{n_{eff}}^2 - {n_s}^2}{{n_f}^2 - {n_{eff}}^2}}\right), \quad (2.8)$$

The dispersion relation for slab waveguide for TM polarized light is given by

$$m\pi = \frac{2\pi}{\lambda} d\sqrt{{n_f}^2 - {n_{eff}}^2} - tan^{-1}\left(\frac{{n_f}^2}{{n_c}^2}\sqrt{\frac{{n_{eff}}^2 - {n_c}^2}{{n_f}^2 - {n_{eff}}^2}}\right) - tan^{-1}\left(\frac{{n_f}^2}{{n_s}^2}\sqrt{\frac{{n_{eff}}^2 - {n_s}^2}{{n_f}^2 - {n_{eff}}^2}}\right), \quad (2.9)$$

where n_c, n_s, and n_f are refractive index for cover, substrate, and film, n_{eff} is the effective refractive index for mth guided mode (m is the order of mode, m= 0,1,2...), λ is the wavelength, and d is the thickness of the film. Guided modes in a dielectric waveguide may exist when

$$max(n_c, n_s) \leq n_f \quad (2.10)$$

For calculating the number of guided modes that can be supported by an Al_2O_3 film on glass substrate for a particular wavelength is given by

$$n_{eff} = n_s \quad (2.11)$$

$$M_{TE} = \lfloor \frac{2}{\lambda} d\sqrt{{n_f}^2 - {n_s}^2} - tan^{-1}\left(\sqrt{\frac{{n_s}^2 - {n_c}^2}{{n_f}^2 - {n_s}^2}}\right) \rfloor, \quad (2.12)$$

$$M_{TM} = \lfloor \frac{2}{\lambda} d\sqrt{{n_f}^2 - {n_s}^2} - tan^{-1}\left(\frac{{n_f}^2}{{n_c}^2}\sqrt{\frac{{n_s}^2 - {n_c}^2}{{n_f}^2 - {n_s}^2}}\right) \rfloor, \quad (2.13)$$

where M_{TE} and M_{TM} is number of guided modes for TE and TM polarized light respectively. Where $\lfloor x \rfloor$ denotes the largest integer that is smaller than or equal to x. The equation (2.12) can be solved numerically for n_{eff} for given guided modes m (= 0 to M_{TE}). Similarly the equation (2.13) can be solved numerically for n_{eff} for given guided modes m (= 0 to M_{TM}). Wavelength 632.8 nm were used for calculating the effective refractive index for Al_2O_3 film on glass substrate. Effective refractive index is calculated for 400 nm, 300 nm, and 200 nm Al_2O_3 film on soda lime glass substrate. The film refractive index and thickness of the film were taken from the fitting results. There was one TE- fundamental mode and one TM-fundamental mode for 400 nm and 300 nm thick Al_2O_3 on soda lime glass glass substrate. 200 nm thick Al_2O_3 film on soda lime glass film support only one TE- fundamental mode and act as a single mode planar waveguide. Figure (2.9) shows the geometry used for calculation of effective refractive index (n_{eff}).

To measure the effective refractive index, prism coupling method was used. The effective refractive index is defined as

$$n_{eff} = n_p sin\left(\beta + sin^{-1}\left(\frac{sin\theta_m}{n_p}\right)\right), \tag{2.14}$$

where n_p is the refractive index of the prism at particular wavelength, β is the prism angle, and θ_m is the angle at which guide mode is excited.

In experiment we have used a He- Ne laser emitting at 632.8 nm. The prism angle is 60.19 degree and the refractive index of the prism is 1.7520. Table 2.4 shows the calculated and experimental measured effective refractive index for 400 nm thick Al_2O_3 film on soda lime glass. Figure (2.11) shows the guided modes for 400 nm and 300 nm thick Al_2O_3 film on soda lime glass.

For loss measurement, the light is collected by multi-mode fiber from the film

Table 2.4: Experimental and calculated effective refractive index for 400 nm thick Al_2O_3 film on soda lime glass at 632.8 nm wavelength.

	Effective refractive Index			
	Experimental		Calculated	
Film Thickness(nm)	TE-Pol	TM-Pol	TE-Pol	TM-Pol
400	1.5765	1.5614	1.5909	1.5745
300	1.5474	1.5289	1.5688	1.5453
200	1.5159	-	1.5264	-

surface along the light track. The intensity of the guided mode was measured as a function of the distance. The intensity profile in waveguide are defined as

$$I = I_0 exp(-\alpha x), \tag{2.15}$$

Where α is losses in waveguide. Losses in dB/cm is defined as

$$\alpha_{dB} = \frac{10}{L} log_{10}(\alpha), \tag{2.16}$$

where L is length in cm traveled by guided mode in the waveguide. Figure (2.12) shows the losses inside the waveguide as a function of distance in millimeters. The slope of intensity curves correspond to the losses in range of 7 dB/cm.

The simple analytical model proposed by Payen et. al. [52] shows that propagation loss α is defined as:

$$\alpha = 0.76 \frac{\lambda \sigma^2}{2\pi (d/2)^4 n_f}, \tag{2.17}$$

where σ is the surface roughness, λ is the wavelength, d is the film thickness, and n_f is the film refractive index. The surface roughness (σ) is $\pm$ 0.3, and film refractive index is 1.68 at 632.8 nm wavelength. The average theoretical propagation losses for our samples is 0.75 dB/cm. The experimental propagation losses is higher than the analytical propagation losses. This is because of the contribution of volume scattering

or porosity in the film.

The propagation losses and refractive index reported by Smit et al. [53] was 25 dB/cm and 1.54 at 633 nm wavelength by r.f. sputtering process and after an annealing process at 800^oC, the refractive index of their alumina film increased from 1.54 to 1.70. The propagation loss decreased from 25 dB/cm to about 1 dB/cm. By ion-beam sputtering [54], the reported propagation loss before annealing at 633 nm was 0.4 - 2.9 dB/cm and after annealing was 0.23 dB/cm. By pulsed laser deposition, the propagation losses at 633 nm was 10 dB/cm [55]. As discussed above, either the propagation losses are too high or it requires high temperature to get good film [56]. But by ALD technique, the propagation loss was 7 dB/cm at 300^oC deposition temperature without any extra step.

2.4 Conclusion

Al_2O_3 was used in integrated optics and usually deposited by PECVD, sputtering, and evaporation technique. To achieve high index step Al_2O_3 with low propagation losses, either deposition is needed to be done on high temperature or annealed at high temperature. On other hand, ALD provides smooth surface with high step index and low propagation losses.

In our study, we showed that Al_2O_3 deposited by atomic layer deposition technique have surface roughness of $\pm$ 0.3 nm with propagation loss of 7 dB/cm. The optical properties were calculated by fitting measured reflection spectrum to the calculated reflection spectrum. The quality of fit was investigated by calculating mean squared error. The refractive index of Al_2O_3 was approx. 1.63 and 1.68 at 632 nm wavelength on silicon, and soda lime glass substrate, respectively. The mean squared error was 0.0008 and 0.0068 for silicon and soda lime glass substrate, respectively.

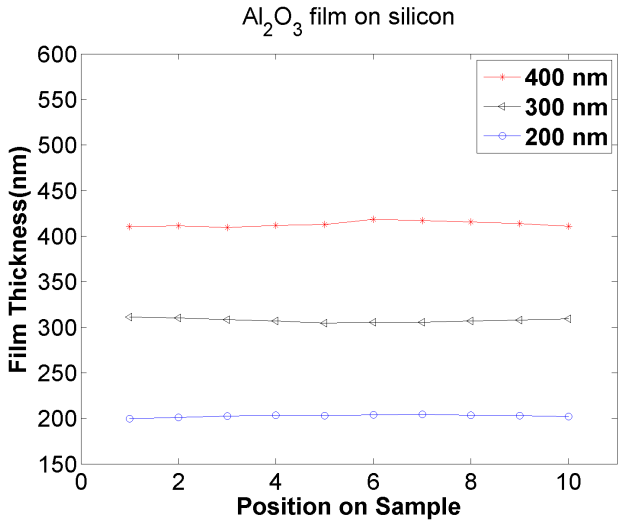

(a)

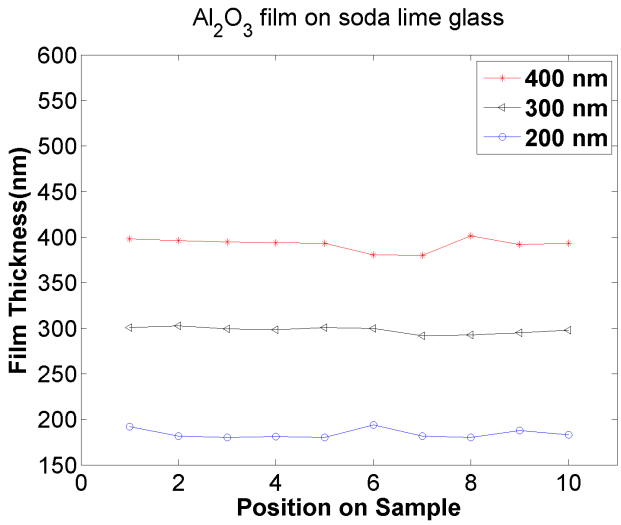

(b)

Figure 2.8: Film thickness of Al_2O_3 on (a) silicon and (b) soda lime glass substrate.

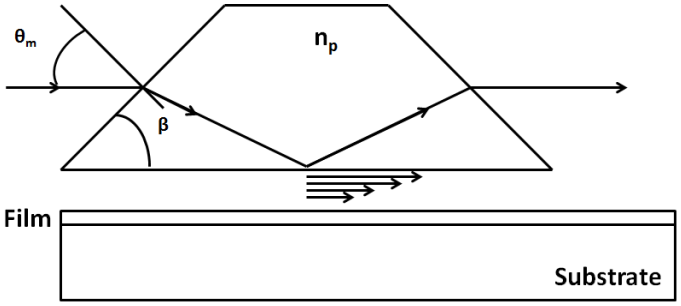

Figure 2.9: Geometry for calculation of effective refractive index by prism coupling method.

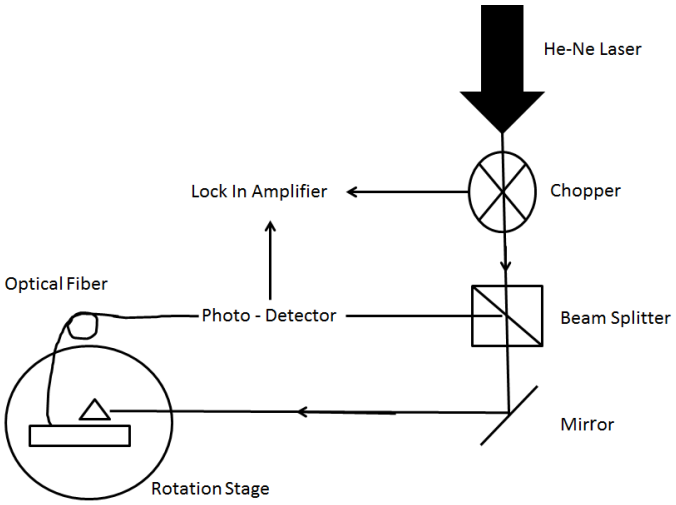

Figure 2.10: Schematic diagram of experiment.

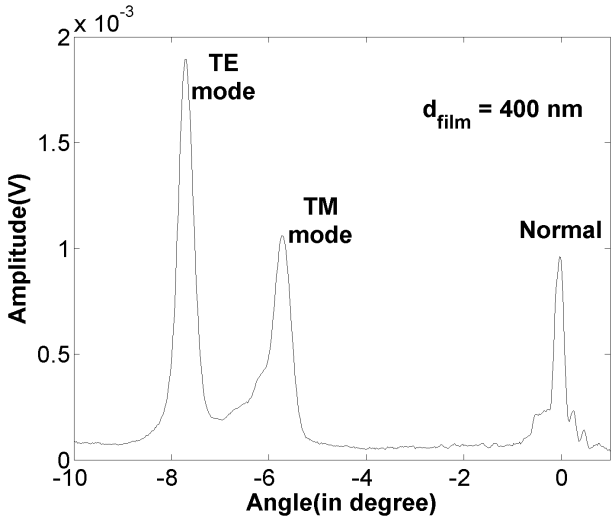

(a)

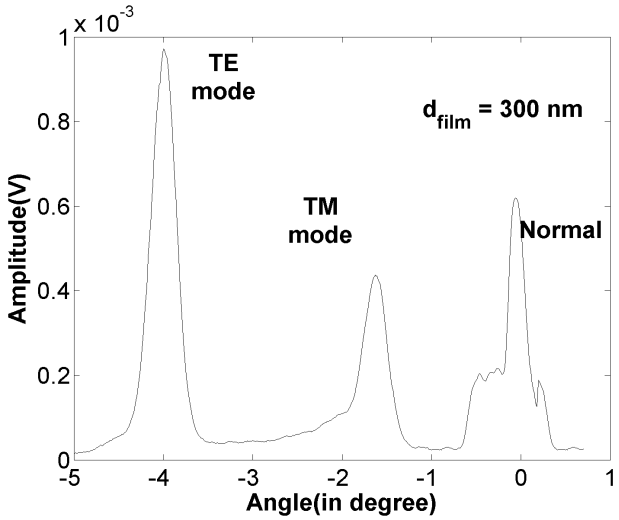

(b)

Figure 2.11: Guided modes excitation for Al_2O_3 film on soda lime glass for (a) 400 nm, (b) 300 nm thick film.

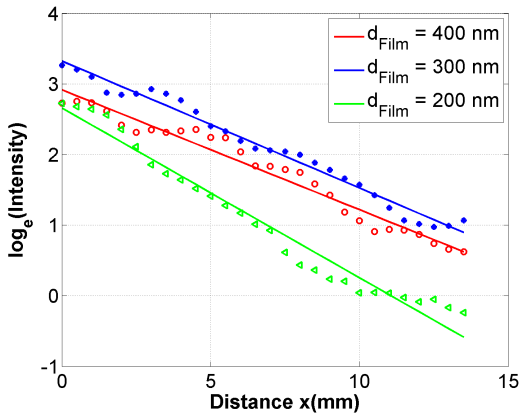

Figure 2.12: Propagation loss for Al_2O_3 film on soda lime glass for 400 nm, 300 nm, and 200 nm thick film at 632.8 nm wavelength.

CHAPTER 3

Waveguide Based Microspectrometer With a Computer Generated Diffractive Optical Element.

3.1 Waveguide Design

Waveguide is the basis of integrated optics and communication channel. As mentioned in chapter 1, waveguide with high index step provides high confinement and can be used in an integrated optical circuits that substitute micro-electronics circuit. The optical waveguide guide the light by total internal reflection at its interface. Optical waveguide is a basis of microspectrometer.

The planar waveguide can be characterized by the film refractive index (n_f), substrate refractive index (n_s), cover refractive index (n_c), and film thickness (d). The relationship between these parameters for TE polarized light is given by equation 3.1

$$d = \frac{\lambda}{2\pi\sqrt{{n_f}^2 - {n_{eff}}^2}} \left(m\pi + tan^{-1}\left(\sqrt{\frac{{n_{eff}}^2 - {n_c}^2}{{n_f}^2 - {n_{eff}}^2}}\right) + tan^{-1}\left(\sqrt{\frac{{n_{eff}}^2 - {n_s}^2}{{n_f}^2 - {n_{eff}}^2}}\right)\right), \tag{3.1}$$

where n_{eff} is the effective refractive index for m^th guided mode (m is the order of mode, $m = 0, 1, 2...$), λ is the wavelength. Single mode optical waveguide is preferred over multi mode waveguide, since angle of diffraction depends upon the effective refractive index and single mode planar waveguide provides one focus per wavelength.

The high index step material is desirable to get strong evanescent field. As mentioned in chapter 1, HfO_2 has high refractive index (≈ 2) and physically strong material. To calculate thickness of HfO_2, we need to solve equation 3.1. For spectral

range 425 nm to 700 nm, 200 nm thick HfO_2 will support one fundamental TE mode and one fundamental TM mode.

3.2 Design of Chirped Waveguide Grating

The design of microspectrometer revolves around diffractive element, collimation or focusing, and detection. In our design, chirped waveguide grating (CWG) was used as diffractive element and focusing. For delivering light to the chirped waveguide grating, planar waveguide has been used. Since angle of diffraction depends upon the effective refractive index, single mode planar waveguide has been used to get one focus per wavelength. For detection, regular CMOS camera was used.

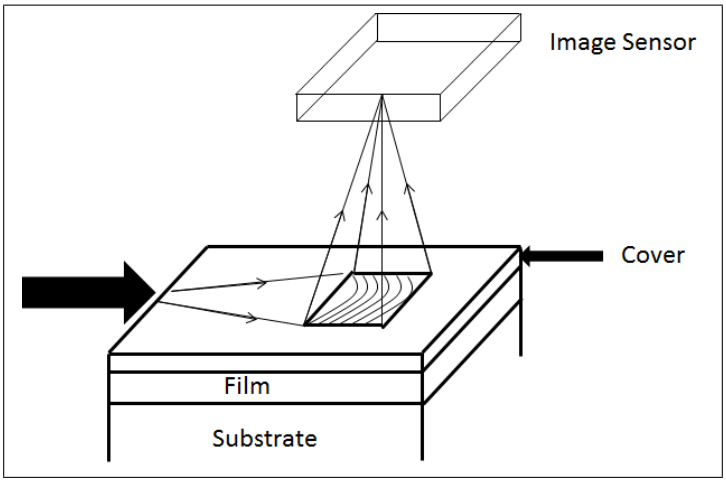

Figure 3.1: The proposed design of microspectrometer.

The design of chirped waveguide grating starts from choice of the center wavelength. Center wavelength (λ_0) is defined as a wavelength which is focused above at the center of grating. The grating period (Λ_0) at the center of grating can be calculated as:

$$\Lambda_0 = \frac{\lambda_0}{n_{eff}(\lambda_0)} \tag{3.2}$$

Dimensions of the chirped waveguide grating plays crucial role in defining the spot size of the focused beam. The determination of size of chirped waveguide grating depends upon the coupling strength and depth of grating [57, 58]. The out-coupled power from the chirped waveguide decreases as it travels along chirped waveguide grating area. Depth of chirped waveguide grating gives the choice to cover whole area of chirped waveguide grating. In order to provide optimal functionality from chirped waveguide grating, we have to optimize length and depth of chirped waveguide grating. Figure (3.2) shows relationship between the length and depth of chirped waveguide grating.

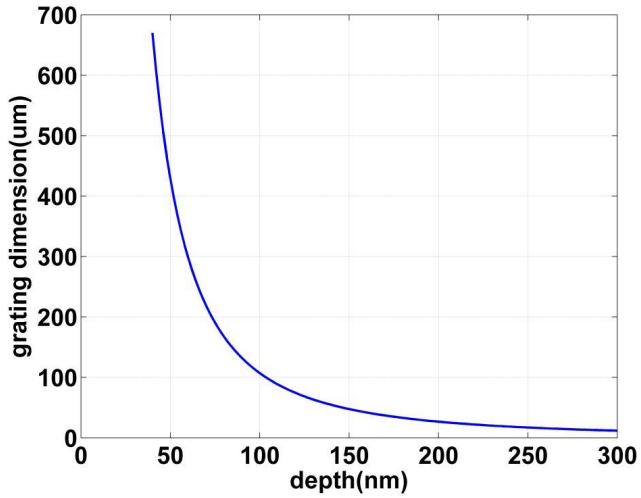

Figure 3.2: Relationship between the length and depth of chirped waveguide grating.

Once we select the central wavelength and size of chirped waveguide grating, we can design the two dimensional groove of chirped waveguide grating. Figure (3.3) shows two dimensional groove of chirped waveguide grating and the curves shows the peak of each groove. The location of peak of each grove can be calculated by estimating total phase (ϕ) accumulated as light travels from source O to the grating

$P(x, y)$ and focus F above at the center of grating. The total phase (ϕ) accumulated form O to F is equal to integer multiple of 2π [36].

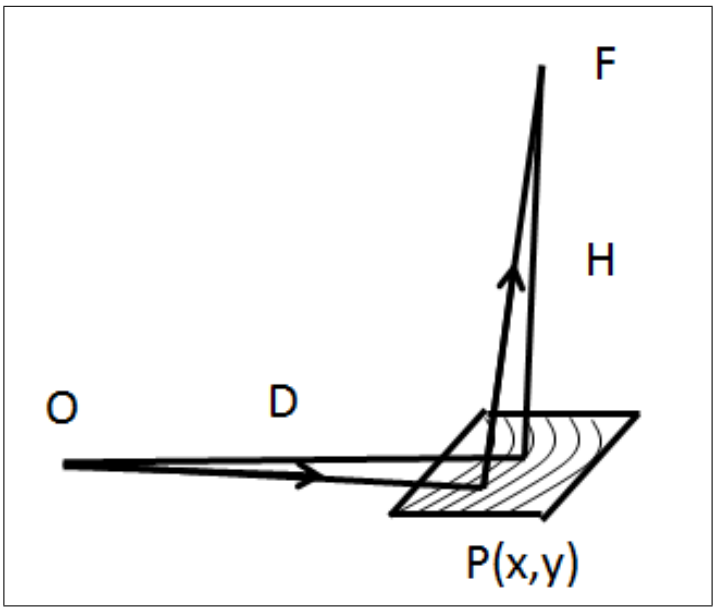

Figure 3.3: Ray diagram of chirped waveguide grating.

$$\phi = \frac{2\pi}{\lambda_0} n_{eff} \sqrt{(D+x)^2 + y^2} + \frac{2\pi}{\lambda_0} n_a \sqrt{x^2 + y^2 + H^2} \tag{3.3}$$

where ϕ is total phase accumulated for each path from O to F, λ_0 is center wavelength, n_{eff} is the effective refractive index at center wavelength, D is the distance from the source point of center of the grating, H is the distance of focal point from center of the grating, x and y define the location of the pixel, and center of chirped waveguide grating is at the origin (0,0).

For other wavelengths the position of the focal point can be approximated using geometrical considerations. The locations of the focal points for different wavelengths will lie along a curved line. For each waveguide mode this curve will be different because the effective refractive index will be different for each mode. Therefore, a

single mode waveguide is required to get one focal point per wavelength. The focal points for each wavelength can be calculated by considering that the small change in distance along the chirped waveguide grating (in say + X-direction) gives a small change in diffraction angle.

$$sin(\theta) = \frac{1}{n_a}\left(n_{eff} - \frac{\lambda}{\Lambda_0}\right) \tag{3.4}$$

$$a_0 = \frac{d}{dx}\left[\frac{1}{\Lambda(x)}\right]_{x=0} \tag{3.5}$$

$$x(\lambda) = \frac{n_a sin(\theta) cos^3(\theta)}{\lambda a_0} \tag{3.6}$$

$$z(\lambda) = \frac{n_a cos^3(\theta)}{\lambda a_0} \tag{3.7}$$

where λ is the wavelength, n_{eff} is the effective refractive index, n_a is the refractive index of the air, θ is the diffracted angle measured with respect to the waveguide plane, Λ_0 is grating period at $x = 0$, and $\Lambda(x)$ is the period of the chirped waveguide grating at x.

Figure (3.4) shows the resulting focal curve for wavelengths from 425 nm to 700 nm, with a 480 nm center wavelength. The origin is at the center of chirped waveguide grating, the position of the focal spot for the center wavelength is 5 mm above the chirped waveguide grating (along the z-axis), and the distance from the source to the center of chirped waveguide grating is 5 mm (along the x-axis).

The design was carried out for visible range and the center wavelength was 480 nm and the dimensions of the chirped waveguide grating was 250 μm x 250 μm. The source point was taken 5 mm and focal point was taken at 5 mm, the refractive index of the HfO_2 film was 1.7211 at 480 nm wavelength. Figure (3.5) shows the chirped waveguide grating layout transfer from Matlab to LASI.

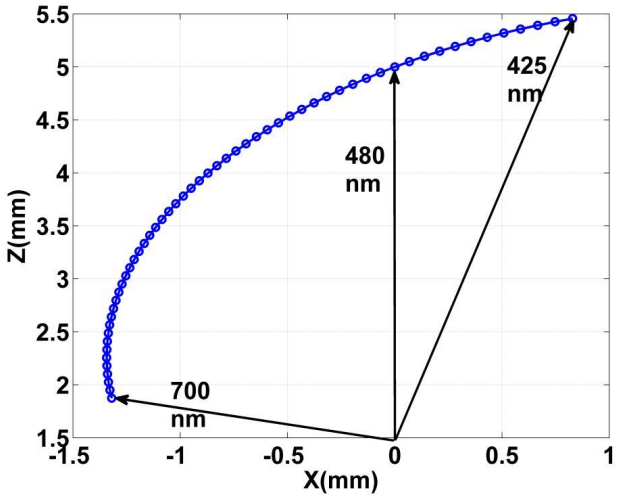

Figure 3.4: The resulting focal curve for 425 nm to 700 nm with $\lambda_0 = 480$ nm.

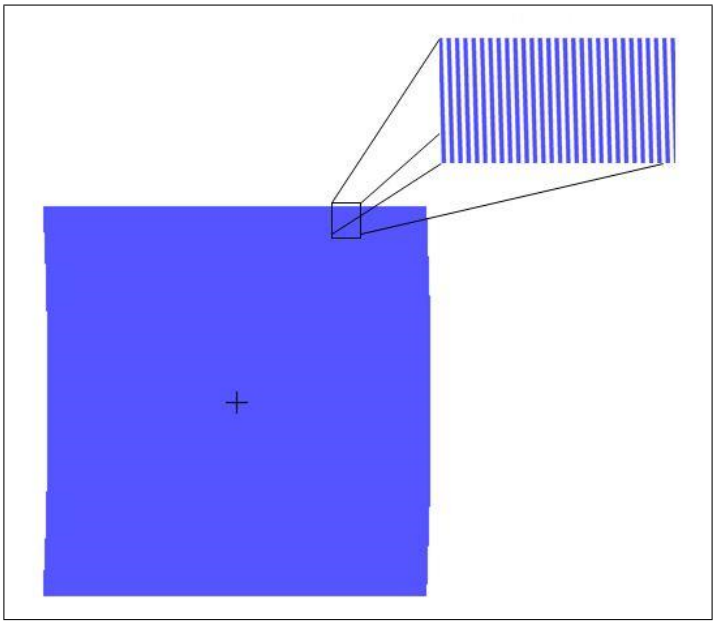

Figure 3.5: The chirped waveguide grating layout transfer from Matlab to LASI.

By calculation the chirped waveguide grating's period was approximately 300 nm at the beginning and decreases as we move away from the source point, but for

particular period the duty cycle was 50%. For E-beam lithography, the L-edit was used to create GDSII file. The calculated diffraction spot size for 250 μm chirped waveguide grating length is 2.09 μm. Figure (3.6) shows the chirped waveguide grating layout for E-beam lithography in L-edit with markers.

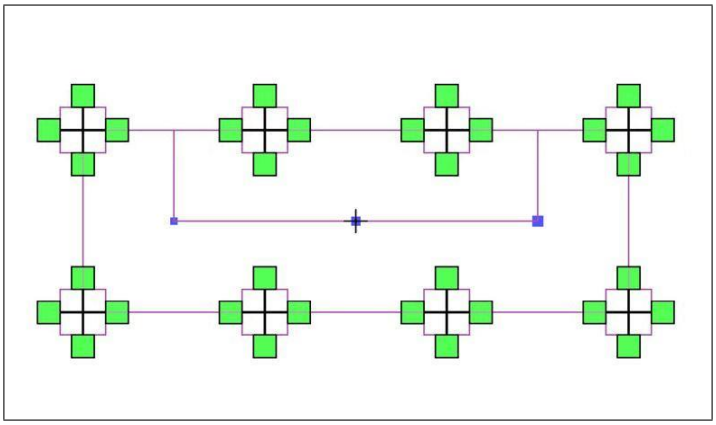

Figure 3.6: The chirped waveguide grating in Ledit.

For designing chirped waveguide gratings, Matlab was used for simulation to make text file. Generated text file was then transferred to the LASI software to make GDSII file. Ledit was used to put together chirped waveguide grating and marker for ebeam lithography.

3.3 Fabrication of Chirped Waveguide Grating

The fabrication was done in Nanofabrication laboratory at Penn State University. Chirped waveguide gratings were fabricated on fused quartz substrates. The waveguide core was formed by depositing a 200 nm thin film of HfO_2 onto the substrate using atomic layer deposition (ALD). The fabrication procedure on HfO_2 of the chirped waveguide grating is described below.

The step involved in ebeam lithography are as follow

1. Cleaning samples
2. SiO_2 deposition
3. O_2 plasma etching
4. Ebeam resist spin coating
5. Soft baking
6. Gold deposition
7. Ebeam writing & design
8. Gold etching & Developing
9. SiO_2 etching
10. Removal of ebeam resist

The sample dimension was 12 mm x 12 mm. Figure (3.7) shows the graphical illustration of ebeam lithography process.

3.3.1 Cleaning Samples

The first step in nano fabrication is to clean sample as much as possible. Even if we can not see the dust particle by eyes, at nano scale it will contributes in scattering losses. We had removed dust particles by using pressurized clean N_2. Then the samples were cleaned for half an hour by acetone using ultra-sonics followed by cleaning by isopropanol for half an hour using ultra-sonic bath.

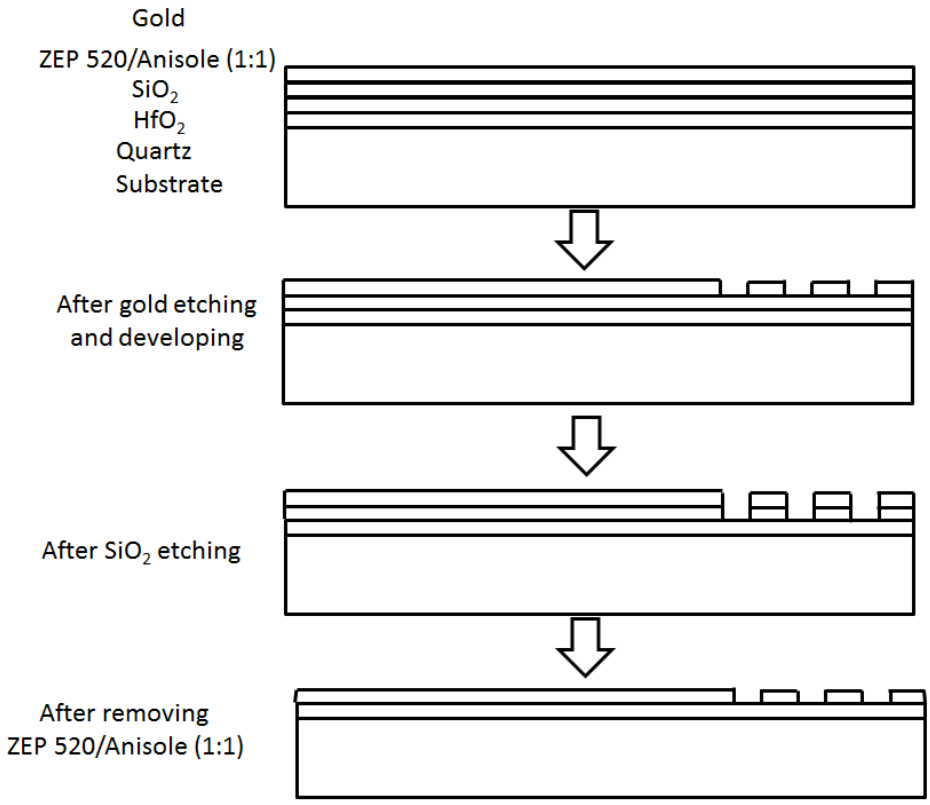

Figure 3.7: Graphical illustration of ebeam lithography process.

3.3.2 SiO_2 Deposition

A 75 nm SiO_2 cladding layer was deposited using plasma enhanced chemical vapor deposition (PECVD). The SiO_2 deposition was done with an Applied Material P-5000 PECVD Cluster tool. The deposition was for 35 seconds at 300^oC and the gas flow rate for the N_2O was 840 sccm, for the SiH_4 it was 20 sccm, and for the N_2 it was 1400 sccm.

3.3.3 O_2 Plasma Etching

To improve adhesion, the samples were cleaned by Nano-strip and then by O_2 plasma. A Metroline M4L Plasma Etcher tool was used for 2 minutes for O_2 plasma cleaning. The gas flow rate was 150 sccm for the O_2 and 50 sccm for the He. The power used was 300 W.

3.3.4 Ebeam Resist Spin Coating

A programmable spinner was used to spin ebeam resist onto the samples. An adjustable vacuum chuck hold the samples inside spinner. To get desired thickness, we need to optimize time and rpm of spinner. ZEP 520/Anisole (1:1), a positive resist, was used for electron beam lithography resist and we have used 2500 rpm for 1 min.

3.3.5 Soft Baking

After spinning the resist on samples, the samples were soft baked at 180^oC for 3 minutes to remove residuals. The thickness of ebeam resist was around 215 nm, measured by profilometer.

3.3.6 Gold Deposition

Since the samples were on quartz substrates, 10 nm gold films were deposited by Kurt Lesker Thermal Evaporator in order to avoid surface charging during ebeam lithography. The deposition rate was 0.5 $\pm$ 0.1 A/sec and the deposition time was 3 min. We got 9 nm $\pm$ 1 nm of gold on top of ebeam resist.

3.3.7 Ebeam Writing & Design

A Leica EBPG5-HR Electron Beam Writer was used to write chirped waveguide grating pattern into the resist. The ebeam lithography process was an iterative process and it needs to be optimize for our application. For example, in ebeam lithography, the exposure dose, thickness of ebeam resist and time are important parameter. To optimize the dose for our sample a dose array matrix was written on quartz sample

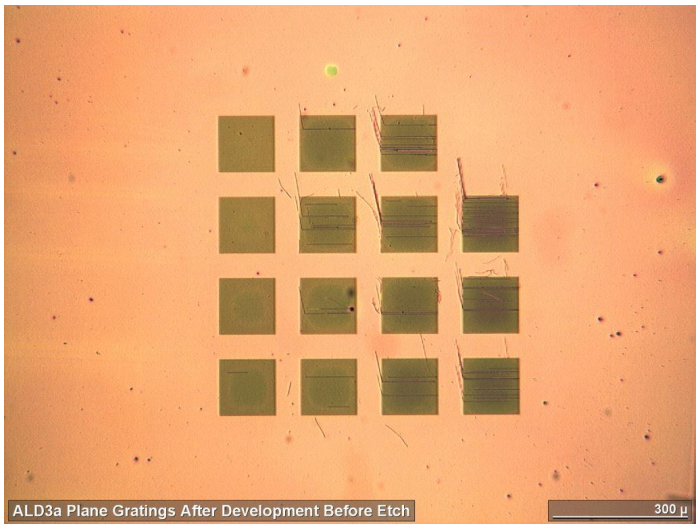

Figure 3.8: Optical microscope image of dose array matrix.

after all previous step.

The dose varies from 150 $\mu c/cm^2$ to 290 $\mu c/cm^2$ with step of 10 $\mu c/cm^2$. Figure (3.8) shows optical microscope image of the dose array matrix for quartz sample. 160 $\mu c/cm^2$ dose was chosen for ebeam lithography and two gratings from dose matrix array have been selected for illustration.

Figure (3.9a) and (3.9b) shows optical microscope image of individual grating from dose array matrix for 160 $\mu c/cm^2$ and 290 $\mu c/cm^2$ dose. From figures it is clear that at dose 160 $\mu c/cm^2$ grating is good and at dose 290 $\mu c/cm^2$ grating was over developed. Figure (3.10a) and (3.10b) shows scanning electron microscope (SEM)

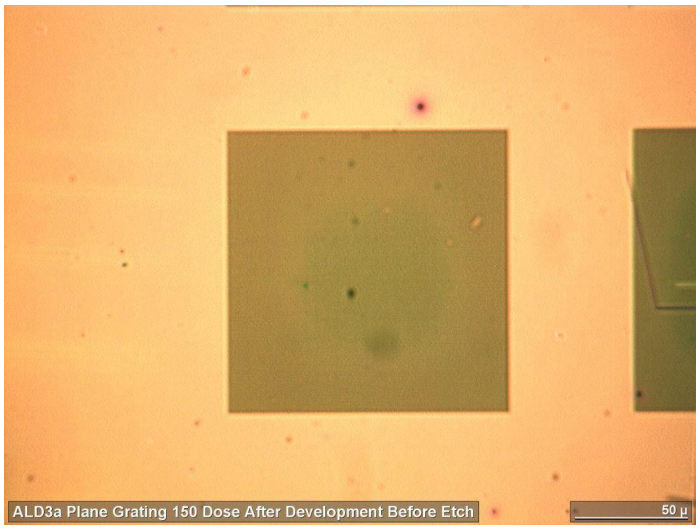

(a)

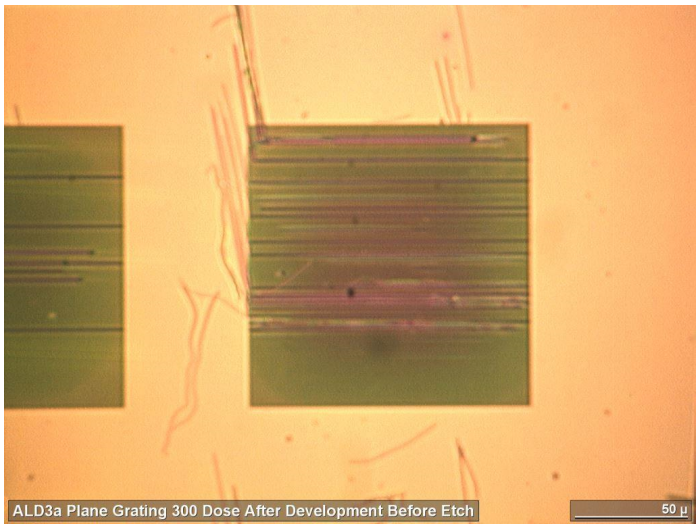

(b)

Figure 3.9: Optical microscope image of individual grating from dose array matrix.(a) dose 160 $\mu c/cm^2$ and (b) dose 290 $\mu c/cm^2$.

image of individual grating from dose array matrix for 160 $\mu c/cm^2$ and 290 $\mu c/cm^2$ dose.

Figure (3.9b) and (3.10b) shows the fail fabrication of chirped waveguide grating. The exposure dose and ebeam resist thickness for this step was 290 $\mu c/cm^2$ and 215 nm. To avoid this kind of failure, either we need to reduce the expousre dose or

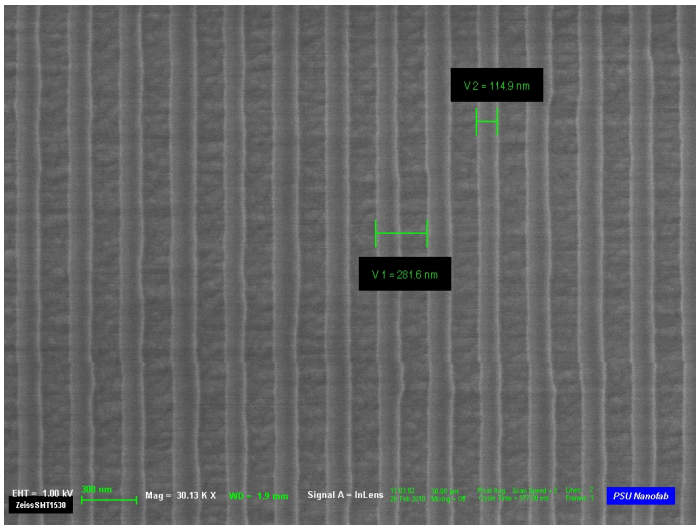

(a)

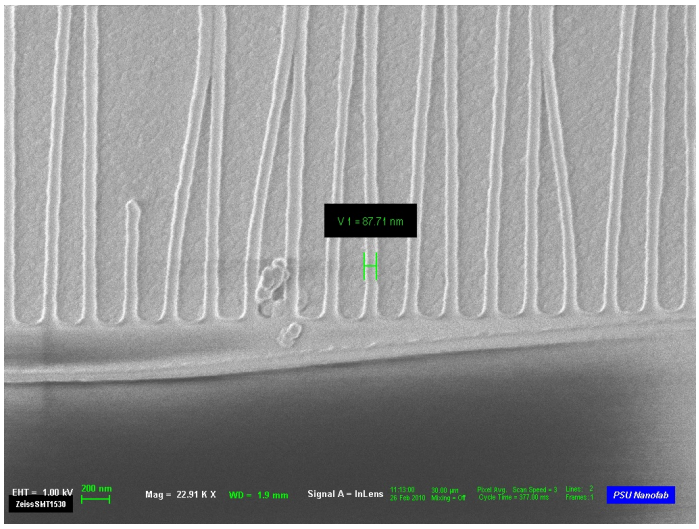

(b)

Figure 3.10: Scanning electrom microscope (SEM) image of individual grating from dose array matrix.(a) dose 160 $\mu c/cm^2$ and (b) dose 290 $\mu c/cm^2$.

increase the ebeam resist thickness.

3.3.8 Gold Etching and Developing

After e-beam writing, the gold film was etched away by a gold etch-type TFA chemical for 30 seconds. The e-beam resist was developed by n-amyl acetate for 3 minutes, the development process was stopped by immersion in MIBK/IPA (8:1) for 30 seconds, and the samples were rinsed with IPA for 30 seconds. Figure (3.11) shows optical microscope image of chirped waveguide grating with markers.

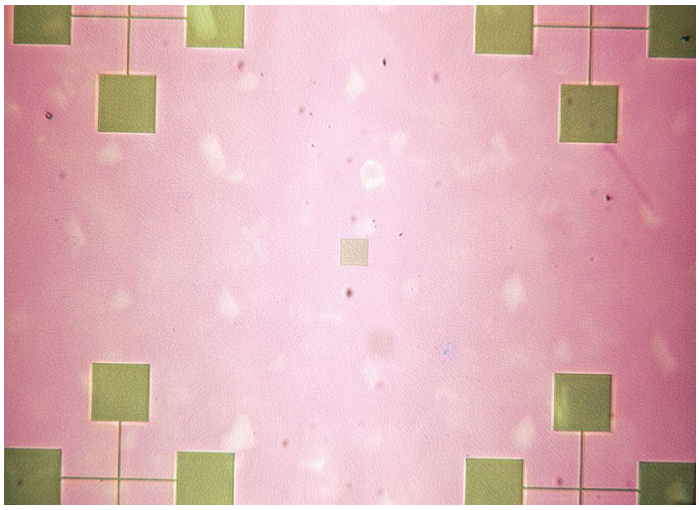

Figure 3.11: The chirped waveguide grating after development with markers.

3.3.9 SiO_2 Etching

An Applied Materials AMAT MARIE was used to etch the pattern into the SiO_2 cladding layer. The etching was done for 180 seconds. The ZEP 520 was striped by using n, n-dimethylactamide for 5 minutes. A Leo 1530 FE-SEM was used to take images of the gratings.

3.4 Experiment and Results

The experiment was done to check the functionality of micro-spectrometer. Light from semi-conductor laser and Ar_+ -ion laser was combined using beam splitters. A microscope objective was used to focus the light at point O and the distance between the source point at O and center of grating was 5 mm. The diverging light from point O is focused by the grating onto the image sensor. The intensity was attenuated to avoid the sensor saturation. Figure (3.12) shows the schematic diagram of our experiment. The wavelengths of the light from two laser sources were 458 nm, and 532.8 nm.

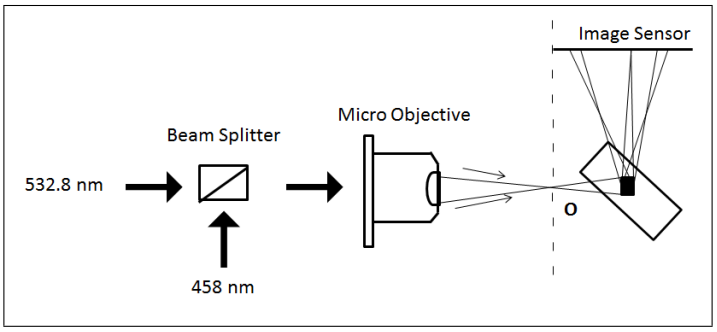

Figure 3.12: Schematic diagram of experiment.

The image of the focused beams was recorded by a CMOS sensor from Pixel link. The pixel size of the sensor array is 6.7 μm x 6.7 μm, frame rate is 25 fps, and the sensing area is 8.6 mm x 6.9 mm. The CMOS sensor was mounted on 3D translation stage and adjusted to bring the light from the 458 nm source into sharp focus on the detector.

Light of wavelength 458 nm was focused at above in the center of the grating and 532.8 nm wavelength light was focused next to right side of 458 nm wavelength as shown in Figure (3.13). Light of wavelength 458 nm gives sharp focus, as CMOS sensor was placed at its focal plan. For 532.8 nm wavelength light, the image was

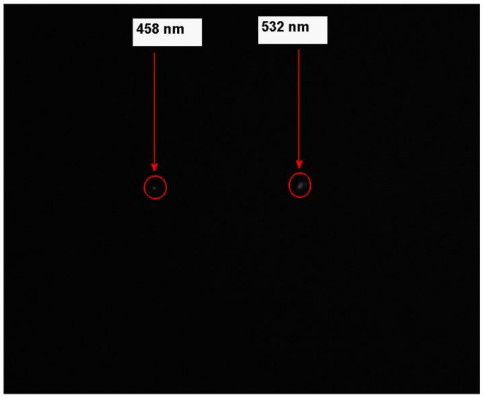

Figure 3.13: Image Recorded by CMOS image sensor.

captured before the focus.

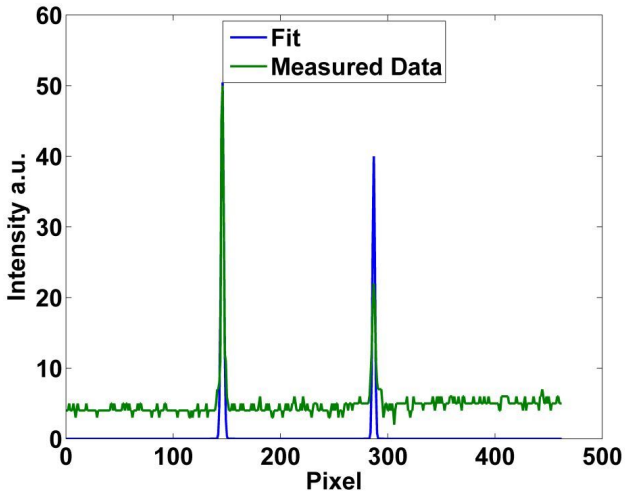

Figure 3.14: The Intensity distribution along a line through the focus light row of pixel.

Figure(3.14) shows the intensity distribution along a line through the focus light row of pixel. The focus points were 2-3 pixels wide at full width half maximum level. The position of peak and full width half maximum was calculated by applying gaussian fit. Figure(3.14) also shows fit intensity distribution.

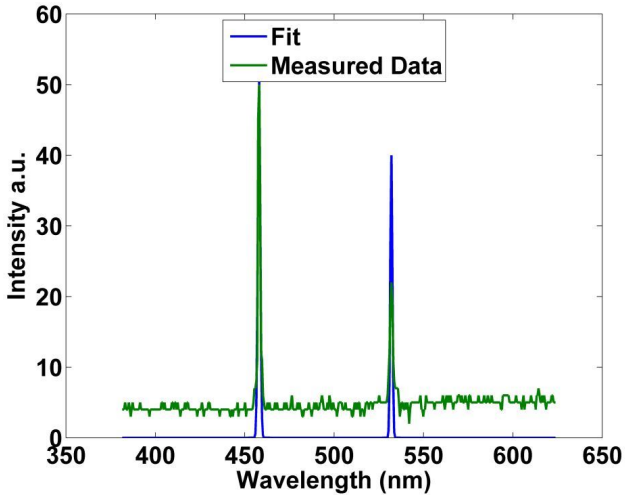

Figure 3.15: The Intensity distribution in wavelength range.

The intensity distribution with respect to pixel was changed to the wavelength range by linear approximation. The slope of the line was calculated by assigning the wavelength to the position of peak. The full width half maximum for 458 nm and 532.8 nm were 2 nm and 3 nm, respectively. Figure(3.15) shows the intensity distribution in wavelength range.

3.5 Conclusions

The combination of free space geometry (micro - optics) has resulted in a compact microspectrometer. This is worth mentioning that the micro-spectrometer size is 12 mm x 12 mm with quick read out property and provide 2.5 nm resolution. Most of the microspectrometers have size in inches with resolution less than 5 nm and if the size is small , resolution is more than 6 nm. As mentioned in Avrutsky et. al. [36], the main draw back of the plan grating and lens based micro-spectrometer is the lens astigmatism of the out coupled radiation. Also device provides 0.3 nm to 4.6 nm of variable resolution with respect to above mention device. The above

microspectrometer is integrated on planar waveguide base and doesn't require any optical scheme for focusing.

Since microspectrometer provides real time spectrum, it is best candidate for in-situ measurement. The planar waveguide base makes it robust and well suited for lab-on-chip application. The compatibility with CMOS technology makes it more flexible to fabricate.

CHAPTER 4

Enhanced Spontaneous Emission Near Waveguide

4.1 Introduction

The implication of the environment affecting the spontaneous emission is that the rate of emission could be suppressed if the atoms are placed in a cavity [59–62] or in a photonic crystal [63] with no modes available at the transition frequency. Alternatively, if the environment provides higher density of states of electromagnetic field compared to that in vacuum, the spontaneous decay becomes faster. The emission rate is relatively easy measured by monitoring lifetime of luminescence excited by short laser pulses, and this aspect of environment-dependent spontaneous emission has been studies extensively [59–67].

Another important aspect is how the emitted radiation is distributed among the available radiation modes. It is implicitly presented in calculations of the spontaneous emission rate as long as the total rate is the sum of emission rates into particular modes. This aspect, however, has not been studies as comprehensively, perhaps, because of its experimental verification is not straightforward. From practical perspective, if the emission is collected using some specific electromagnetic modes, the efficiency of spontaneous emission coupling to these modes becomes an important factor in deciding the performance of the system under investigation. In particular, on-chip integrated microsystems may use optical waveguides to transmit the emission from the substance being analyzed to the spectral sensor. If emission directed into the guided modes is efficient enough, it eliminates necessity for additional optical elements such as mirrors and micro-lenses designed for collecting light radiated into

free space and coupling it to the waveguide.

It has been found that a high-index waveguide film provides additional radiative channels and thus enhances the emission rate. In this study we are specifically interested in the efficiency of the process, namely, the percentage of spontaneously emitted radiation power that is captured by the guided modes. To be close to a practically important configuration, we presume that liquid analyte is flowing in a microfluidic channel right above a planar waveguide. The surface of the waveguide is functionalized to specifically adsorb the molecules of interest, which then produces fluorescence, being excited by external radiation (Fig. 1). The adsorbed molecules are then placed in close proximity to the waveguide surface. The medium above the guiding film in this case is mainly water or alcohol or other solvents that delivers the analyte. It is also possible that the liquid is removed from the channel, so that the top medium is filled with air.

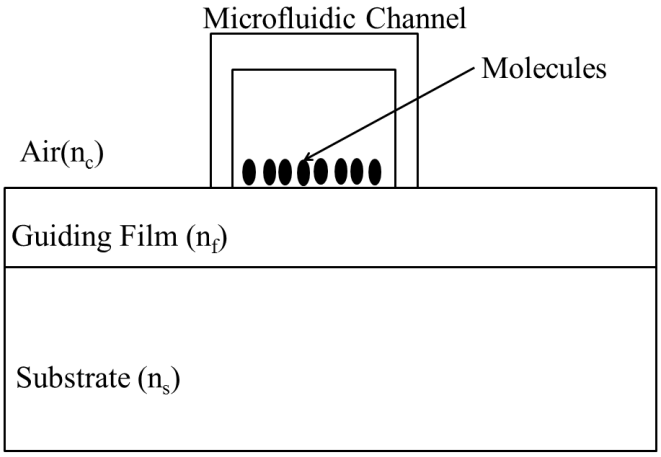

Figure 4.1: Illustration of the quantum emitter near waveguide.

4.2 Theoretical Formalism

if an atom is sitting on top of a film at distance z, the spontaneous emission rate W is given by

$$W = \frac{2\pi e^2}{\hbar^2 c}|D_{12}|^2 F(z), \tag{4.1}$$

where $\hbar$ is the plank constant, c is the speed of light in vacuum, e is the electron charge, D_{12} is the dipole matrix element of the atomic transition, and $F(z) = (F^x(z)+F^y(z)+F^z(z))/3$ is the zero-point electromagnetic field fluctuation for random orientation of the atomic dipole moment, where $F^j(j = x, y, z)$ is jth component of zero-point electromagnetic field fluctuation. Here, the dipole matrix element is assumed to have no preferential orientation. Figure 4.2 shows the quantum emitter (an atom or a molecule) at distance z from waveguide surface.

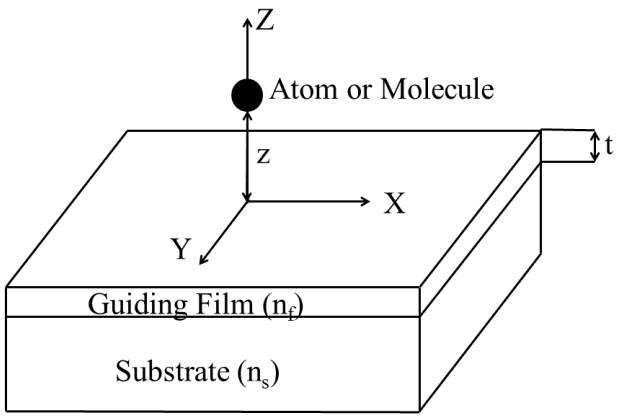

Figure 4.2: The general View of an atom or a molecule at distance z from waveguide surface.

For this system the zero-point electromagnetic field fluctuation can be written as sum of the contribution in radiation modes $F_R{}^j(z)$ and guided modes $F_G{}^j(z)$ and

can be calculate by

$$F_R{}^j(z) = \sum_{p=TE,TM}\sum_{\mu=Sub}^{Cover}\int_0^{2\pi}\int_0^{k_0 n_\mu}\frac{\hbar\omega_0}{2\epsilon_0}|E^j_{kp\mu}(\vec{r})|^2\beta d\beta d\phi, \quad (4.2)$$

$$F_G{}^j(z) = \sum_{p=TE,TM}\sum_{\substack{\nu\geq 1\\ k_\nu^{p,min}<k_0}}\int_0^{2\pi}\frac{\hbar\omega_0}{2\epsilon_0}|E^j_{kp\nu}(\vec{r})|^2\beta^p_\nu(\vec{k_0})\frac{d\beta^p_\nu}{dk}(k_0)d\phi, \quad (4.3)$$

where ϵ_0 is the permitivitty in vacuum; $k_0 = \omega_0/c$ is the wave number of the emission light in vacuum; $E(\vec{r})$ is the electric field at the position of quatum emitter for various modes. TE (TM) indicates the TE (TM) polarization, whose electric (magnetic) field vector is parallel to (x,y) plane; $k = (\beta cos(\phi), \beta sin(\phi), k_{\mu z})$, $k_{\mu z} = \sqrt{(k_0^2 n_\mu^2 - \beta^2)}$, μ represent the substrate and cover surface; ν represent the number of guided modes. If quantum emitter is sitting in a homogeneous dielectric medium with refractive index n, then the components of the zero-point electromagnetic field fluctuation will be

$$F^x = F^y = F^z = nF_{free}, \quad (4.4)$$

$$F_{free} = \frac{\hbar{\omega_0}^3}{6\pi^2\epsilon_0 c^2}, \quad (4.5)$$

where ω_0 is the angular frequency of spontaneous emission, and ϵ_0 is the permittivity of the vacuum. Since the relative spontaneous emission rate W/W_{free} is equal to the normalized zero-point electromagnetic field fluctuation F/F_{free}, so to simplify we will follow normalized zero-point electromagnetic field fluctuation, where W and W_{free} are the atomic spontaneous emission rates in medium and in vacuum, respectively, F and F_{free} are zero-point electromagnetic field fluctuation in medium and in vacuum, respectively

The coupling efficiency $\eta(z)$ can be calculated as a ratio of normalized zero-point electromagnetic field fluctuation of total guided modes $F_G(z)$ to the total normalized zero-point electromagnetic field fluctuation $F(z)$. Equation (4.6) and (4.7) give total normalized zero-point electromagnetic field fluctuation and coupling efficiency, respectively.

$$F_G(z) = \frac{1}{3} \sum_{j=x,y,z} {F_G}^j(z) \tag{4.6}$$

$$F(z) = \frac{1}{3} \sum_{j=x,y,z} {F_G}^j(z) + {F_R}^j(z) \tag{4.7}$$

$$\eta(z) = \frac{F_G(z)}{F(z)} \tag{4.8}$$

4.3 Dependence of coupling efficiency on the refractive index of the film

Using the above model we have studied how efficiency of coupling to the guided modes depend upon the film thickness and refractive index. The substrate and cover refractive index (n_s and n_c respectively) are assumed to be 1.0; film refractive index(n_f) is varied from 1.01 to 2.5, and film thickness is equal to 0.1λ and 1λ, where λ is the emission wavelength. For thickness $t = 0.1\lambda$ waveguide support only one TE mode and one TM mode for refractive index from 1.01 to 2.5. For film thickness 1λ waveguide support three TE and TM modes, when film refractive index is 1.5, and five TE and TM modes, when the film refractive index is 2.5. The coupling efficiency depends upon film refractive index and thickness of the film. For 0.1λ thick waveguide, as film refractive index increases, the coupling efficiency increases as the film refractive index increases. As the film thickness increases from 0.1λ to 1λ, the coupling efficiency increases. By varying refractive index, the number of modes increases and so the coupling efficiency.

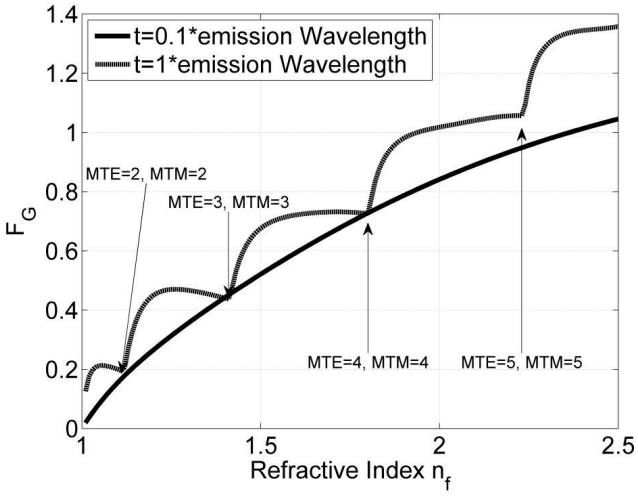

(a)

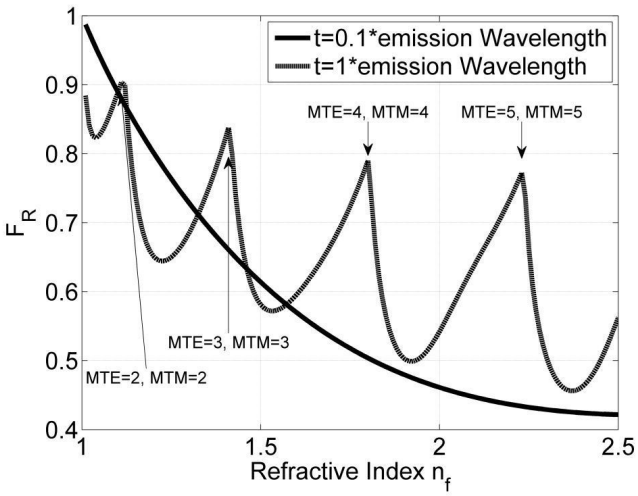

(b)

Figure 4.3: The normalized zero-point field fluctuation as a function of film refractive index.(a) Guided Mode and (b) Radiation Mode.

Figure (4.3a), (4.3b) shows the zero-point field fluctuation for guided mode and radiation mode as a function of film refractive index, the emission wavelength is assumed to be 530 nm. The two film thicknesses are 53.0 nm, and 530 nm. Figure (4.3a) shows, as a new mode introduced the zero-point field fluctuation increases and then it becomes constant. Figure (4.4) shows the coupling efficiency as a function of

film refractive index. As the refractive index of thin film is increased, the coupling efficiency increases. Our calculation is in good agreement with Urbach et. al [44]. MTE and MTM represents number of modes for TE and TM polarization respectively.

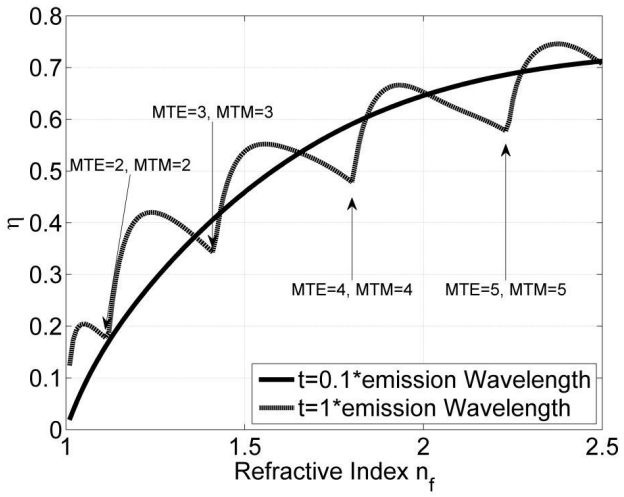

Figure 4.4: The coupling efficiency as a fuction of film refractive index.

From geometric optics point of view, if we have assumed that the atom is sitting inside the waveguide, then the coupling efficiency depends upon the critical angle between the film and the substrate and given by $\eta = \sqrt{\frac{{n_f}^2 - {n_s}^2}{{n_f}^2}}$. Figure (4.5) shows the coupling efficiency of an excited atom by assuming the radiation is isotropic in space, and the film captures all the rays approaching the interfaces at angles exceeding the critical angle for total internal reflection. The difference between the above model and geometrical optics calculation arises because the light inside the waveguide is carried by guiding modes, not by rays.

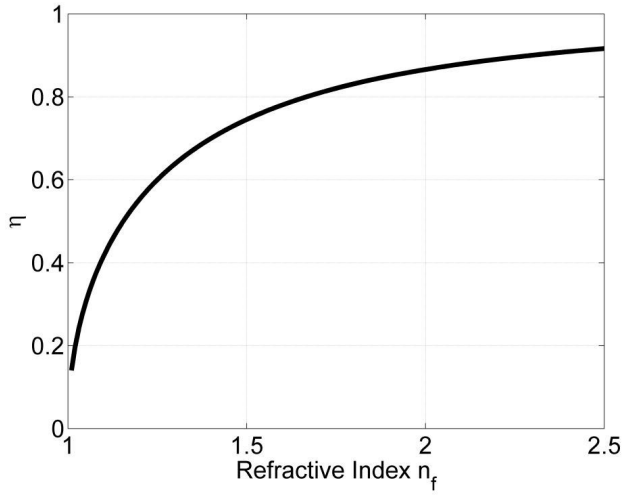

Figure 4.5: The coupling efficiency as a function of film refractive index.

4.4 Dependence of coupling efficiency on the location of the emitter

The above model is applied for Al_2O_3, and silicon nitride (SiN) thin film on soda lime glass. The emission wavelength is 530 nm, the thickness of thin film is 0.4λ. The coupling efficiency increase as it approaches the waveguide boundary. If atom is placed on the surface of waveguide, the coupling efficiency is approximately 0.30 for Al_2O_3, and SiN thin film on soda lime glass respectively. Since most of the dye dissolve in alcohol, the two configuration are taken into account for cover: air and alcohol. Figure (4.6), and (4.7) shows coupling efficiency as a function of $2z/t$ for air/Al_2O_3, alcohol/Al_2O_3, air/SiN, and alcohol/SiN on soda lime glass respectively. The thin film thickness is 212.0 nm. As shown in graph the efficiency increases as the atom approaches to the waveguide surface and goes down to zero within 1.33 um of distance from surface of waveguide. Thus if an fluorescent molecules are absorbed at the surface of the waveguide, the significant amount of light will be captured by waveguide. The standalone silicon membrane performs same way, provided that

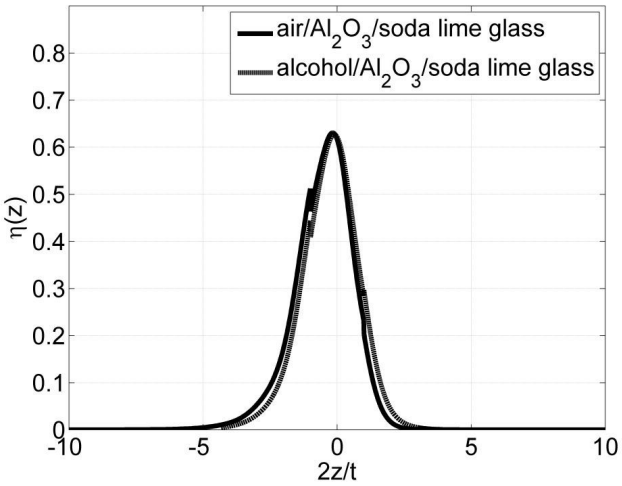

Figure 4.6: The coupling efficiency as a function of $2z/t$ for air/Al_2O_3 and alcohol/Al_2O_3 on soda lime glass.

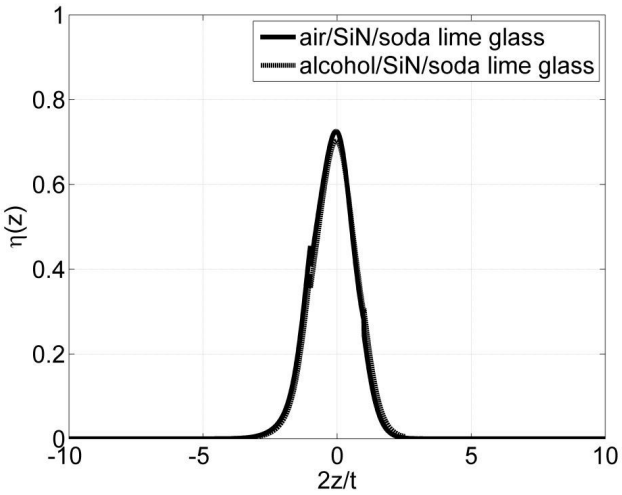

Figure 4.7: The coupling efficiency as a function of $2z/t$ for air/SiN and alcohol/SiN on soda lime glass.

emission takes place in infrared region. The efficiency of light collection by silicon membrane approaches 0.90. The emission wavelength is 1550 nm, the refractive index of cladding is considered as 1, refractive index of silicon membrane is considered 3.47, and the membrane thickness is 310 nm. Figure (4.8) shows the coupling efficiency as a

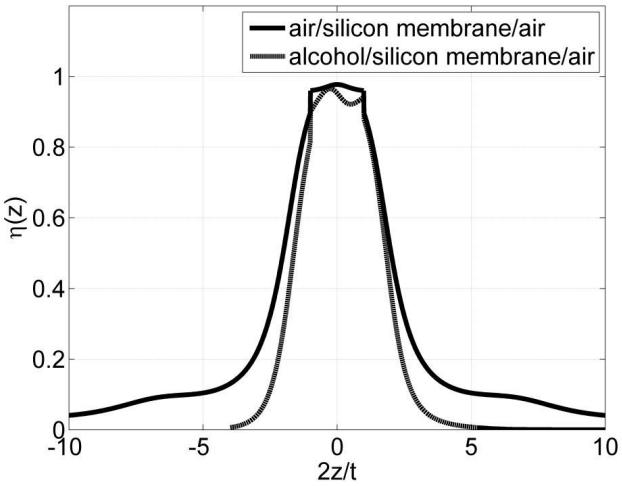

Figure 4.8: The coupling efficiency as a function of $2z/t$ of air/silicon membrane and alcohol/silicon membrane.

function of $2z/t$ for air/silicon membrane, and alcohol/silicon membrane respectively.

4.5 Dependence of coupling efficiency on Dipole element matrix of an atom

The coupling efficiency also depends upon the orientation of a dipole matrix element. The most interesting case is when an atoms have dipole matrix element orthogonal to the surface of a waveguide. In this case radiation happens along waveguide surface and there is no radiation along dipole element matrix or perpendicular to the waveguide surface. The coupling efficiency of such system is given by

$$\eta^z(z) = \frac{{F^z}_G(z)}{{F^z}_G(z) + {F^z}_R(z)}, \tag{4.9}$$

where ${F^z}_G(z)$ and ${F^z}_R(z)$ represents zero-point field fluctuation of guided modes and radiation modes, respectively, if dipole element matrix is orthogonal to surface of waveguide. Since we have only TM modes, the electric field components are dis-

continued at the waveguide surface due to boundary condition and we observe a jump in zero-point field fluctuation of guide mode if an atom is at the surface of a waveguide. Figure (4.9a), and (4.9b) shows normalized zero-point field fluctua-

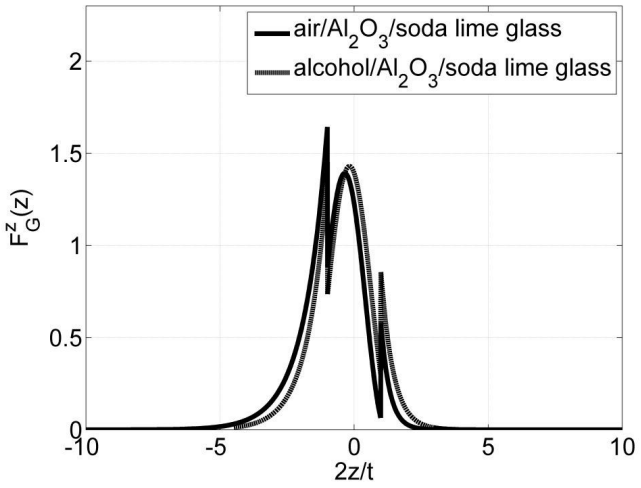

(a)

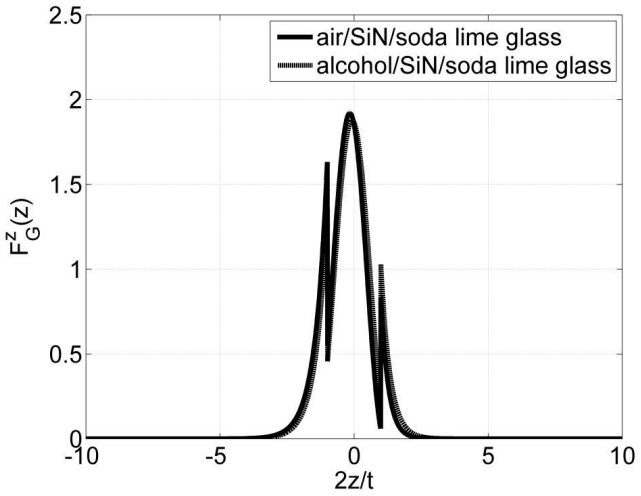

(b)

Figure 4.9: The normalized zero field fluctuation of guide modes as a function of $2z/t$. (a) air/Al_2O_3 and alcohol/Al_2O_3 (b) air/SiN and alcohol/SiN on soda lime glass.

tion of guided modes as a function of $2z/t$ for air/Al_2O_3, alcohol/Al_2O_3, air/SiN,

and alcohol/SiN on soda lime glass respectively. Figure (4.10a), and (4.10b) shows normalized zero-point field fluctuation of radiation modes as a function of $2z/t$ for air/Al_2O_3, alcohol/Al_2O_3, air/SiN, and alcohol/SiN on soda lime glass respectively.

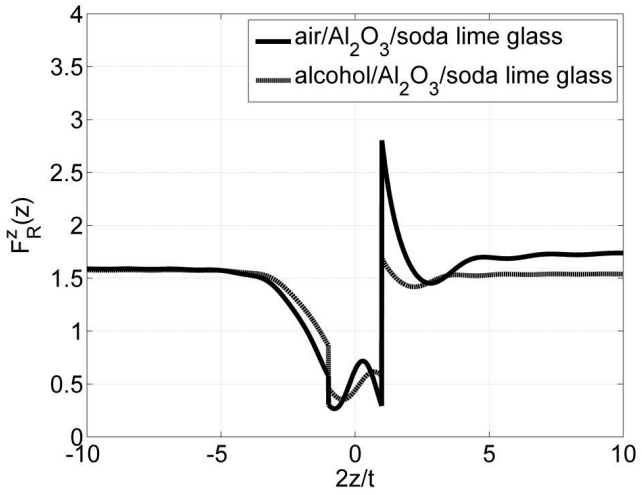

(a)

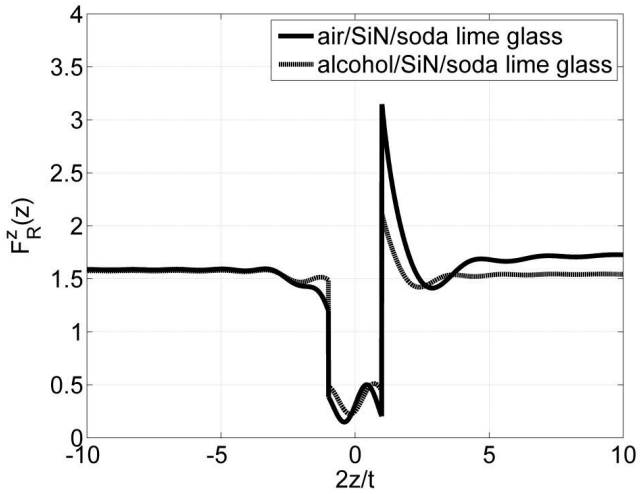

(b)

Figure 4.10: The normalized zero-point field fluctuation of radiation modes as a function of $2z/t$. (a) air/Al_2O_3 and alcohol/Al_2O_3 (b) air/SiN and alcohol/SiN on soda lime glass.

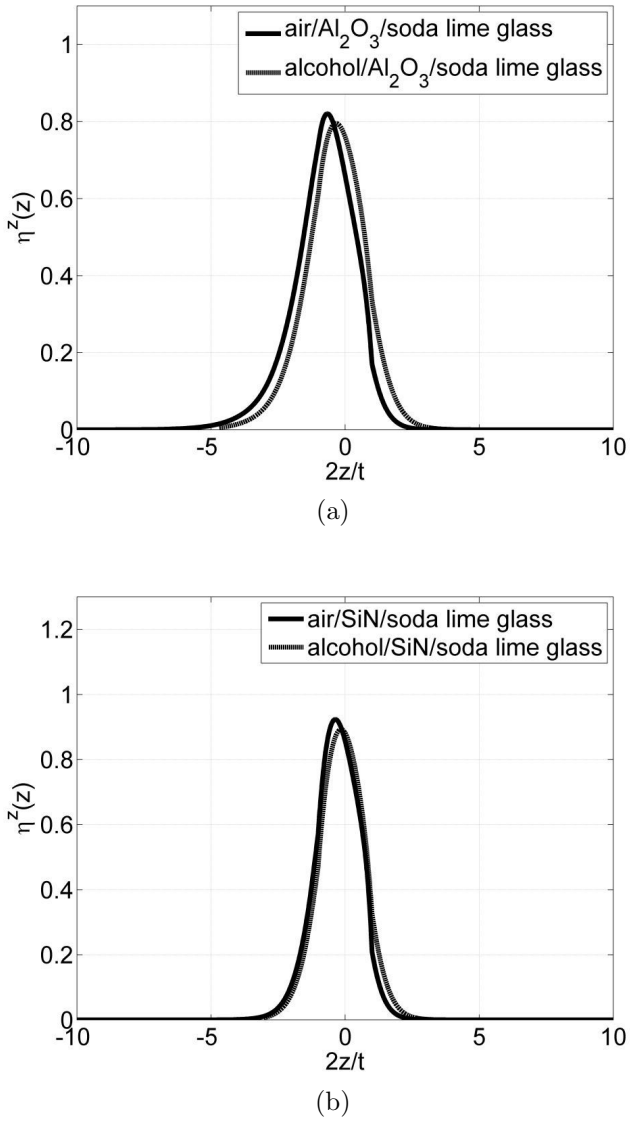

Figure 4.11: The coupling efficiency as a function of $2z/t$. (a) air/Al_2O_3 and alcohol/Al_2O_3 (b) air/SiN and alcohol/SiN on soda lime glass.

Figure (4.11a), and (4.11b) shows coupling efficiency as a function of $2z/t$ for air/Al_2O_3, alcohol/Al_2O_3, air/SiN, and alcohol/SiN on soda lime glass respectively, if the dipole matrix is orthogonal to the waveguide surface. The coupling efficiency will increase by factor of a 2 and this is because the atom emits light only in xy plane and there is no emission in z direction.

4.6 Conclusion

The spontaneous emission of an atom is related to the density of state(DOS), DOS of a medium is directly proportional to the refractive index of the material. The DOS and spontaneous emission rate increases as atom enters in the vicinity of the waveguide. The number of guided modes depends upon the difference of film refractive index and the substrate refractive index. As the difference increases, the number of guided modes increase and more light guided through the waveguide. As we see, the coupling efficiency increases in order from Al_2O_3, SiN, through silicon membrane.

In conclusion, we have studied efficiency of spontaneous light emission into guided modes of a thin film. We shown that fluorescence of molecules absorbed at the surface of the waveguide is coupled to the guided modes with efficiency comparable to the case when emitter is placed inside of a film. we have also shown that in case of dipole matrix element orthogonal to the plane of the waveguide, the efficiency can be order of magnitude higher if the molecules are absorbed at the surface compared to the case of when emitters are inside of a film.

CHAPTER 5

Conclusion

The optical and waveguide properties of Al_2O_3 deposited by atomic layer deposition technique was investigated. The quality of the surface was better than other deposition technique. The surface roughness of Al_2O_3 film was approx. ± 0.3 nm over film thickness of 400 nm, 300 nm, and 200 nm measured by atomic force microscope. Atomic layer deposition provides uniform thickness over entire sample. The film thickness was calculated by measuring reflection spectrum at ten different points. The average film thickness for Al_2O_3 film on silicon substrate was 413.15$\pm$5 nm, 307.61$\pm$5 nm, and 202.50$\pm$5 nm for targeted film thickness 400 nm, 300 nm, and 200 nm, respectively. The average film thickness for Al_2O_3 film on soda lime glass substrate was 392.27$\pm$10 nm, 297.85$\pm$7 nm, and 184.08$\pm$5 nm for targeted film thickness 400 nm, 300 nm, and 200 nm, respectively. The propagation loss was 7 dB/cm for 632.8 nm wavelength.

The microspectrometer of size 12 mm x 12 mm was fabricated by using optical waveguide as a base. Its spectral resolution was 2.5 nm in spectral range of 425 nm - 700 nm, which is better than existing microspectrometer. The careful design of diffractive optical element was demonstrated by using Matlab, LASI, and Ledit. This microspectrometer is integrated in a planar optical waveguide and will become good base for fabrication of micro-fluidic channels. There is a good scope to build a lab on a chip with this design for bio-sensors and chemical sensors. Micro-fluidic channel can be used to transport analyte to the optical waveguide surface and the optical signature of analyte can be analyses by using microspectrometer.

The coupling efficiency of a quantum emitter was investigated and is directly

related to the refractive index of the film and position of quantum emitter with respect to the surface of waveguide. The coupling efficiency for Al_2O_3, SiN, and stand alone silicon membrane was calculated. If quantum emitter was placed on the surface of planar waveguide, it will emit 30% of radiation into the guided mode for Al_2O_3, SiN thin film on soda lime glass. The most interesting case was related to the orientation of dipole element matrix. If an atom or molecule has dipole matrix element orthogonal to the surface of planar waveguide, then the coupling efficiency of such system is more as compared to the atom or molecule placed inside the film layer. The calculated coupling efficiency was approx. 60% for Al_2O_3, SiN thin film on soda lime glass.

REFERENCES

[1] George I. Stegeman, and Colin T. Seaton, Nonlinear integrated optics, Journal of applied physics 58.12 (1985): R57-R78.

[2] E. J. Murphy, Integrated optical circuits and components: Design and applications, CRC PressI Llc, 1999.

[3] Feng Chen, Xue-Lin Wang, and Ke-Ming Wang, Development of ion-implanted optical waveguides in optical materials: A review, Optical materials 29.11 (2007): 1523-1542.

[4] O. Heavens, Optical Properties of Thin Solid Films1991: Dover Publications.

[5] J. Voros, J. Ramsden, G. Csucs, I. Szendro, S. De Paul, M. Textor, N. Spencer, Optical grating coupler biosensors, Biomaterials, 23 (2002) 3699-3710.

[6] Y. Noda, M. Suzuki, Y. Kushiro, S. Akiba, High-speed electroabsorption modulator with strip-loaded GaInAsP planar waveguide, Journal of Lightwave Technology, 4 (1986) 1445-1453.

[7] F. Pang, X. Han, F. Chu, J. Geng, H. Cai, R. Qu, Z. Fang, Sensitivity to alcohols of a planar waveguide ring resonator fabricated by a solgel method, Sensors and Actuators B: Chemical, 120 (2007) 610-614.

[8] R.N. Ghosh, J. Shmulovich, C.F. Kane, M.R. de Barros, G. Nykolak, A.J. Bruce, P.C. Becker, 8-mV threshold Er/sup 3+/-doped planar waveguide amplifier. Photonics Technology Letters, IEEE 8.4 (1996): 518-520.

[9] R.H. French, H. Mllejans, D.J. Jones, Optical Properties of Aluminum Oxide: Determined from Vacuum Ultraviolet and Electron Energy Loss Spectroscopies, Journal of the American Ceramic Society, 81 (1998) 2549-2557.

[10] F. Ay, J. Bradley, R. de Ridder, K. Worhoff, M. Pollnau, Bragg gratings in Al_2O_3 channel waveguides by focused ion beam milling, in: Proceedings Symposium IEEE/LEOS Benelux Chapter. University of Twente, 2008.

[11] J. Mackenzie, G. Murugan, A. Yu, J. Abshire, Er-doped planar waveguides for power amplifier applications, in: SPIE LASE, International Society for Optics and Photonics, 2013, pp. 859908-859908-859906.

[12] K. Worhoff, J. Bradley, F. Ay, M. Pollnau, Low-loss Al2O3 waveguides for active integrated optics, in: Conference on Lasers and Electro-Optics, Technical Digest, 2007.

[13] C. Laurent-Lund, M. R. Poulsen, M. Beukema, J.E. Pedersen, PECVD grown multiple core planar waveguides with extremely low interface reflections and losses, Photonics Technology Letters, IEEE, 10 (1998) 1431-1433.

[14] Y. Kim, S. Lee, C. Park, S. Lee, M. Lee, Substrate dependence on the optical properties of AlO films grown by atomic layer deposition, Applied Physics Letters, 1997. 71: p. 3604.

[15] P. Raisanen, M. Ritala, and M. Leskel, Atomic layer deposition of Al2O3 films using AlCl 3 and Al (O i Pr)3 as precursors, Journal of Materials Chemistry, 2002. 12(5): p. 1415-1418.

[16] A. Ott, J. Klaus, J. Johnson, S. George, Al3O3 thin film growth on Si (100) using binary reaction sequence chemistry, Thin Solid Films, 292 (1997) 135-144.

[17] S. Najafi, T. Touam, R. Sara, M. Andrews, M. Fardad, Sol-gel glass waveguide and grating on silicon, Journal of Lightwave Technology, 16 (1998) 1640-1646.

[18] H. Im, N.C. Lindquist, A. Lesuffleur, S.-H. Oh, Atomic layer deposition of dielectric overlayers for enhancing the optical properties and chemical stability of plasmonic nanoholes, Acs Nano, 4 (2010) 947-954.

[19] K. Okamoto, Fundamentals of optical waveguides, Academic press, 2010.

[20] K.T. H. Kumagai, M. Matsumoto, and M. Obara, Comparision study of Al2O3 optical crystalline thin films grown by vapor combination of Al(CH3)3/N2O and Al(CH3)3/H2O2, Japnees Journal of Applied Physics, 32 (1993) 6137.

[21] J.H. Correia, G. De Graaf, M. Bartek, R.F. Wolffenbuttel, A single-chip CMOS optical microspectrometer with light-to-frequency converter and bus interface, Solid-State Circuits, IEEE Journal of, 37 (2002) 1344-1347.

[22] R.F. Wolffenbuttel, State-of-the-art in integrated optical microspectrometers, Instrumentation and Measurement, IEEE Transactions on, 53 (2004) 197-202.

[23] D. Sander, J. Mller, Selffocussing phase transmission grating for an integrated optical microspectrometer, Sensors and Actuators A: Physical, 88 (2001) 1-9.

[24] D.S. Goldman, P. White, N. Anheier, Miniaturized spectrometer employing planar waveguides and grating couplers for chemical analysis, Applied optics, 29 (1990) 4583-4589.

[25] S. Ura, F. Okayama, K. Shiroshita, K. Nishio, T. Sasaki, H. Nishihara, T. Yotsuya, M. Okano, K. Satoh, Planar reflection grating lens for compact spectroscopic imaging system, Applied optics, 42 (2003) 175-180.

[26] A.M. del Hierro, W. Kronberger, P. Hietz, I. Offenthaler, H. Richter, A new method to determine the oxygen concentration inside the sapwood of trees, Journal of experimental botany, 53 (2002) 559-563.

[27] C.H. Mazel, Diver-operated instrument for in situ measurement of spectral fluorescence and reflectance of benthic marine organisms and substrates, Optical Engineering, 36 (1997) 2612-2617.

[28] C.P. Bacon, Y. Mattley, and R. DeFrece, Miniature spectroscopic instrumentation: Applications to biology and chemistry, Review of Scientific instruments, 75, 1-16 (2004).

[29] M. Varasi, M. Signorazzi, A. Vannucci, J. Dunphy, A high-resolution integrated optical spectrometer with applications to fibre sensor signal processing, Measurement Science and Technology, 7 (1996) 173.

[30] H. Stiebig, D. Knipp, S.R. Bhalotra, H.L. Kung, D.A. Miller, Interferometric sensors for spectral imaging, Sensors and Actuators A: Physical, 120 (2005) 110-114.

[31] G. Lammel, S. Schweizer, P. Renaud, Microspectrometer based on a tunable optical filter of porous silicon, Sensors and Actuators A: Physical, 92 (2001) 52-59.

[32] O. Manzardo, H.P. Herzig, C.R. Marxer, N.F. de Rooij, Miniaturized time-scanning Fourier transform spectrometer based on silicon technology, Optics letters, 24 (1999) 1705-1707.

[33] S. Kong, D. Wijngaards, R. Wolffenbuttel, Infrared micro-spectrometer based on a diffraction grating, Sensors and Actuators A: Physical, 92 (2001) 88-95.

[34] P. Cheben, I. Powell, S. Janz, D.X. Xu, Wavelength-dispersive device based on a Fourier-transform Michelson-type arrayed waveguide grating, Optics letters, 30 (2005) 1824-1826.

[35] Korablev, O., J-L. Bertaux, A. Grigoriev, E. Dimarellis, Yu Kalinnikov, A. Rodin, C. Muller, and D. Fonteyn. An AOTF-based spectrometer for the studies of Mars atmosphere for Mars Express ESA mission, Advances in Space Research 29, no. 2 (2002): 143-150.

[36] I. Avrutsky, K. Chaganti, I. Salakhutdinov, G. Auner, Concept of a miniature optical spectrometer using integrated optical and micro-optical components, Applied optics, 45 (2006) 7811.

[37] K. Chaganti, I. Salakhutdinov, I. Avrutsky, G. Auner, A simple miniature optical spectrometer with a planar waveguide grating coupler in combination with a plano-convex lens, Optics Express, 14 (2006) 4064-4072.

[38] E. M. Purcell, Physical Review 69, 681 (1946).

[39] D. Axelrod, Cell-substrate contacts illuminated by total internal reflection fluorescence, The Journal of cell biology, 89 (1981) 141-145.

[40] X. Fan, I.M. White, S.I. Shopova, H. Zhu, J.D. Suter, Y. Sun, Sensitive optical biosensors for unlabeled targets: A review, Analytica chimica acta, 620 (2008) 8-26.

[41] X. Fan, I.M. White, Optofluidic microsystems for chemical and biological analysis, Nature photonics, 5 (2011) 591-597.

[42] Y. Yang, A Tunable 3D Optofluidic Waveguide. Oxford: Oxford University Press, 2011.

[43] C. Yeh, Applied Photonics, Bristol: Cengage Learning, 2004.

[44] H. Urbach, G. Rikken, Spontaneous emission from a dielectric slab, Physical Review A, 57 (1998) 3913.

[45] A. I. Baz, B. Zeldovich, and A. M. Peremolov, Scattering, Reactions and Decays in Nonrelativistic Quantum Mechanics. Boston, MA: AMACOM, 2001.

[46] J. P. Dowling, Evanescent Light-wave Atom Mirrors and Resonators, London: CRC Publishers, 2008.

[47] W. Barnes, Fluorescence near interfaces: the role of photonic mode density, journal of modern optics, 45 (1998) 661-699.

[48] S. Brorson, H. Yokoyama, E. Ippen, Spontaneous emission rate alteration in optical waveguide structures, Quantum Electronics, IEEE Journal of, 26 (1990) 1492-1499.

[49] W. Zakowicz, M. Janowicz, Spontaneous emission in the presence of a dielectric cylinder, Physical Review A, 62 (2000) 013820.

[50] R.L. Puurunen, Surface chemistry of atomic layer deposition: A case study for the trimethylaluminum/water process, Journal of applied physics, 97 (2005) 121301-121301-121352.

[51] K. Tadanaga, N. Katata, T. Minami, Super water repellent Al2O3 coating films with high transparency, Journal of the American Ceramic Society, 80 (1997) 1040-1042.

[52] F. Payne, J. Lacey, A theoretical analysis of scattering loss from planar optical waveguides, Optical and Quantum Electronics, 26 (1994) 977-986.

[53] M. Smit, G. Acket, C. Van Der Laan, Al2O3 films for integrated optics, Thin Solid Films, 138 (1986) 171-181.

[54] S. Arnold, B. Cole, Ion beam sputter deposition of low loss Al2O3 films for integrated optics, Thin Solid Films, 165 (1988) 1-9.

[55] A. Suarez-Garcia, J. Gonzalo, C.N. Afonso, Low-loss Al2O3 waveguides produced by pulsed laser deposition at room temperature, Applied Physics A, 77 (2003) 779-783.

[56] M.M. Aslan, N.A. Webster, C.L. Byard, M.B. Pereira, C.M. Hayes, R.S. Wiederkehr, S.B. Mendes, Low-loss optical waveguides for the near ultra-violet and visible spectral regions with Al2O3 thin films from atomic layer deposition, Thin Solid Films, 518 (2010) 4935-4940.

[57] D.L. Zhang, Y. Zhang, Y.M. Cui, C.H. Chen, E. Pun, Long period grating in/on planar and channel waveguides: A theory description, Optics & Laser Technology, 39 (2007) 1204-1213.

[58] A. Katzir, A. Livanos, J. Shellan, A. Yariv, Chirped gratings in integrated optics, Quantum Electronics, IEEE Journal of, 13 (1977) 296-304.

[59] R.G. Hulet, E.S. Hilfer, D. Kleppner, Inhibited spontaneous emission by a Rydberg atom, Physical review letters, 55 (1985) 2137-2140.

[60] D. Kleppner, Inhibited spontaneous emission, Physical review letters, 47 (1981) 233-236.

[61] F. De Martini, M. Marrocco, P. Mataloni, L. Crescentini, R. Loudon, Spontaneous emission in the optical microscopic cavity, Physical Review A, 43 (1991) 2480.

[62] E. Yablonovitch, T. Gmitter, R. Bhat, Inhibited and enhanced spontaneous emission from optically thin AlGaAs/GaAs double heterostructures, Physical review letters, 61 (1988) 2546-2549.

[63] E. Yablonovitch, Inhibited spontaneous emission in solid-state physics and electronics, Physical review letters, 58 (1987) 2059-2062.

[64] S. John, T. Quang, Spontaneous emission near the edge of a photonic band gap, Physical Review A, 50 (1994) 1764.

[65] E. Petrov, V. Bogomolov, I. Kalosha, S. Gaponenko, Spontaneous emission of organic molecules embedded in a photonic crystal, Physical review letters, 81 (1998) 77-80.

[66] M. Megens, H. Schriemer, A. Lagendijk, W.L. Vos, Comment on spontaneous emission of organic molecules embedded in a photonic crystal, Physical review letters, 83 (1999) 5401-5401.

[67] Y. S. Zhou, X. H. Wang, B. Y. Gu, F. H. Wang, Switching control of spontaneous emission by polarized atoms in two-dimensional photonic crystals, Physical review letters, 96 (2006) 103601.

ABSTRACT

ENHANCED SPONTANEOUS EMISSION AND SPECTRAL ANALYSIS USING WAVEGUIDE BASED DEVICES.

by

PRADEEP KUMAR

August 2013

Advisor: Dr. Ivan Avrutsky

Major: Electrical Engineering

Degree: Doctor of Philosophy

Waveguide is one of the basic components of integrated optics and optoelectronics. It consists of a substrate and a high refractive index thin film which confines and directs light. Strong light confinement in a thin film is needed for many applications. For instance, in sensors strong confinement provides high sensitivity, in integrated optical circuits that complement or in some cases substitute micro-electronic circuits strong light confinement allows for smaller footprint of optoelectronic devices. In this dissertation we study optical properties of high-index step waveguides fabricated by atomic layer deposition and their use in a waveguide-based microspectrometer employing a computer-generated diffractive optical element, and explore feasibility of enhancing efficiency of spontaneous emission of individual atoms into guided modes of a high-index waveguide.

Aluminum Oxide (Al_2O_3) is a widely used material in micro-electronics. It is cost effective, and the necessary raw materials are widely available. Atomic layer deposition (ALD) is expected to provide atomic scale smoothness of the film surface as well as low porosity of the film and, as a result, superior quality of optical waveg-

uides. However, because of low growth rate, there are only limited studies of ALD waveguides. We report optical properties of ALD alumina films grown on soda lime and silicon substrates.

Strong light confinement in a high index step waveguide is critical for achieving high resolution in a small footprint waveguide-based microspectrometer. Here we describe design, fabrication, and testing of a diffractive imaging microspectrometer implemented using an ALD HfO_2. Spectral resolution of 2 nm across the entire visible range from 425 nm to 700 nm is achieved in a device with optical components only a few millimeters across.

We also investigated spontaneous emission of atoms placed in close proximity of a high-index planar waveguide. It has been found that a high-index waveguide film provides additional radiative channels and thus enhances the emission rate. The quantum electrodynamics was applied to calculate coupling efficiency of spontaneous emission into the guided modes of the film. The case of special interest is when the dipole matrix element of the transition of interest happens to be orthogonal to the waveguide surface. We found that this configuration may provide improved efficiency of coupling spontaneous emission into the guided modes of the film.

AUTOBIOGRAPHICAL STATEMENT

Pradeep Kumar received his Bachelor of Science in Physics from A. M. U. in Aligarh, Uttar Pardesh, India in May 2002. After finishing his Bachelors, he pursued Master of Science in Physics at Indian Institute of Technology Roorkee and graduated in May 2004. He did many projects related to the photonics, optical trapping of atom, fabrication of waveguide during his master study. He then started his Ph.D. research work in opto-electric devices in elcetrical engineering at Wayne State University under the guidance of Dr. Ivan Avrutsky. He authored and co-authored 3 journal and conference proceedings papers and presented 3 conferences. He is a member of Optical Society of America and The Internation Society for Optics and Photonics. He expects to graduate in May 2013.